NASA TECHNICAL NOTE

NASA TN D-8026

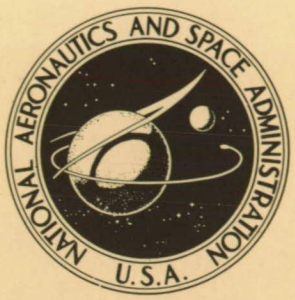

NASA TN D-8026

MOTION-BASE SIMULATOR STUDY OF CONTROL OF AN EXTERNALLY BLOWN FLAP STOL TRANSPORT AIRCRAFT AFTER FAILURE OF AN OUTBOARD ENGINE DURING LANDING APPROACH

David B. Middleton, George J. Hurt, Jr.,
Hugh P. Bergeron, James M. Patton, Jr.,
Perry L. Deal, and Robert A. Champine

Langley Research Center
Hampton, Va. 23665

NATIONAL AERONAUTICS AND SPACE ADMINISTRATION • WASHINGTON, D. C. • OCTOBER 1975

1. Report No.	2. Government Accession No.	3. Recipient's Catalog No.
NASA TN D-8026		

4. Title and Subtitle	5. Report Date
MOTION-BASE SIMULATOR STUDY OF CONTROL OF AN EXTERNALLY BLOWN FLAP STOL TRANSPORT AIRCRAFT AFTER FAILURE OF AN OUTBOARD ENGINE DURING LANDING APPROACH	October 1975
	6. Performing Organization Code

7. Author(s)	8. Performing Organization Report No.
David B. Middleton, George J. Hurt, Jr., Hugh P. Bergeron, James M. Patton, Jr., Perry L. Deal, and Robert A. Champine	L-9743
	10. Work Unit No. 504-09-31-01
9. Performing Organization Name and Address NASA Langley Research Center Hampton, Va. 23665	11. Contract or Grant No.
	13. Type of Report and Period Covered Technical Note
12. Sponsoring Agency Name and Address National Aeronautics and Space Administration Washington, D.C. 20546	14. Sponsoring Agency Code

15. Supplementary Notes

16. Abstract

A moving-base simulator investigation of the problems of recovery and landing of a STOL aircraft after failure of an outboard engine during final approach has been made. The approaches were made at 75 knots along a 6^{o} glide slope. The engine was failed at low altitude and the option to go around was not allowed. The aircraft was simulated with each of three control systems, and it had four high-bypass-ratio fan-jet engines exhausting against large triple-slotted wing flaps to produce additional lift. A virtual-image out-the-window television display of a simulated STOL airport was operating during part of the investigation. Also, a simple heads-up flight director display superimposed on the airport landing scene was used by the pilots to make some of the recoveries following an engine failure.

The results of the study indicated that the variation in visual cues and/or motion cues had little effect on the outcome of a recovery, but they did have some effect on the pilot's response and control patterns.

17. Key Words (Suggested by Author(s))
STOL handling qualities
Motion-base simulation
Engine-out recovery
Motion washout
Heads-up flight director
Externally blown flap

18. Distribution Statement
Unclassified – Unlimited

Subject Category 05

19. Security Classif. (of this report)	20. Security Classif. (of this page)	21. No. of Pages	22. Price*
Unclassified	Unclassified	60	$4.25

*For sale by the National Technical Information Service, Springfield, Virginia 22161

MOTION-BASE SIMULATOR STUDY OF CONTROL OF AN EXTERNALLY BLOWN FLAP STOL TRANSPORT AIRCRAFT AFTER FAILURE OF AN OUTBOARD ENGINE DURING LANDING APPROACH

David B. Middleton, George J. Hurt, Jr., Hugh P. Bergeron,
James M. Patton, Jr., Perry L. Deal,
and Robert A. Champine
Langley Research Center

SUMMARY

A moving-base simulator investigation of the problems of recovery and landing of a short take-off and landing (STOL) aircraft after failure of an outboard engine during final approach has been made. The approaches were made at 75 knots along a 6° glide slope and the engine was failed at altitudes of from 38 to 152 m (125 to 500 ft). The pilots were not given the option to go around. The aircraft was simulated with each of three control systems, and it had four high-bypass-ratio fan-jet engines exhausting against large triple-slotted wing flaps to produce additional lift. A virtual-image out-the-window television display of a simulated STOL airport was used during part of the investigation. A simple heads-up flight director display was also superimposed on the airport scene and used during some of the recoveries.

The results of the study indicated that rather sophisticated stability and control systems were required to assist the pilot in maintaining precise control of this airplane after failure of an engine. (Considerable augmentation was also required for normal four-engine landings.) For the "fully augmented" airplane the motion environment affected control very little because very little motion occurred except in turbulence. As the degree of stability and control augmentation was reduced, serious pilot-induced oscillations (PIO's) sometimes resulted from lateral upsets such as strong side gusts or the failure of an engine. These PIO's occurred in both moving-base and fixed-base runs (made for comparison). The initial motion cues following a disturbance felt realistic and assisted the pilot in making rapid and efficient control corrections, but whenever the input-output relationship developed into an oscillatory mode, the PIO tendency became reinforced by lags in the simulation system. In such cases the lags caused the motion to feel unrealistic and thus degraded the fidelity of the simulation.

When the televised airport scene was added to the simulation, the engine-out (EO) recoveries were often performed more slowly than those that were under strictly instru-

ment conditions. Consequently, maximum excursions from the glide slope and localizer were usually greater, but the recoveries were no less successful. The pilots explained that the gross visual cues from the television (TV) picture reassured them that adequate control of the aircraft was being maintained during the EO transient and recovery and that sufficient time (or distance) remained for unhurried realinement with the runway. When a simple heads-up flight director display was superimposed on the airport scene, the EO recoveries were again performed quickly. The pilots said, however, that in this situation they fixated only on the heads-up director information and tended to ignore the underlying visual scene until the aircraft was under good control and well on its way back to the approach path.

INTRODUCTION

Recent interest in medium-range transport aircraft which can operate out of small airfields has prompted consideration of several aircraft configurations which can produce relatively high lift coefficients at low speeds. For example, during a recent study (ref. 1) the landing speed of a Boeing 707 was reduced approximately 25 percent by use of a powered-lift system in which engine-bleed, compressed air was blown over the upper surface of the wing flaps. This condition made it possible to use flap deflections of 70^{o} as compared with 40^{o} for plain flaps without boundary-layer control. Handling qualities (particularly those associated with lateral motions) deteriorated noticeably at the lowered speed, and several types of stability augmentation were added or recommended. A second method of producing high lift at low speeds is with an externally blown flap (EBF) system where the exhausts from the aircraft's turbofan engines are blown directly against large slotted wing flaps. The failure of one of the outboard engines while in this high-lift configuration, however, will cause significant lift asymmetries as well as thrust vector asymmetries. Consequently, the resulting rolling and yawing moments may create a transient control problem if the handling qualities of the aircraft are not particularly good at low speeds.

The "engine-out" (EO) problems of a conceptual EBF short take-off and landing (STOL) aircraft have been studied analytically, in the wind tunnels (refs. 2 and 3), and in a fixed-base simulation study (ref. 4) at the Langley Research Center. It was determined (ref. 4) that the low-speed handling qualities of the basic airplane would be poor and considerable augmentation would be required in order to obtain a satisfactory pilot rating in both normal and EO situations. However, it was still not known how the presence of cockpit motion might affect the piloting task during EO transients; therefore, the present investigation was undertaken. It was expected that the difficulty of the EO control task would be reduced because the motion environment would provide useful natural cues, and

that good control could be maintained in normal situations with a much simpler stability and control augmentation system than that used in the fixed-base simulation.

The computer program of the fixed-base study (ref. 4) was adapted to the Langley real-time dynamic simulator (RDS) for a motion study of the EO problem during 6^{o} glide-slope landing approaches at 75 knots. The aerodynamics and control systems were thus essentially the same for both studies and the RDS cockpit controls and instrument displays were arranged like those of the fixed-base cockpit. A virtual-image television scene of a typical STOL airport was used during part of the study. (This same airport scene had been used but presented in a slightly different manner in the study of reference 4. Also, the same pilots that participated in the reference 4 study flew the approaches (using the same techniques) and made the handling-qualities evaluations.

SYMBOLS

In order to facilitate international usage of the data presented, dimensional quantities are presented in both the International System of Units (SI) and U.S. Customary Units. The measurements and calculations were made in U.S. Customary Units. Dots over symbols denote differentiation with respect to time.

A,B,C,D,E	computer model internal gains
a_{ij}	direction-cosine elements of inertial-to-body transformation matrix ($i = 1, 2, 3$; $j = 1, 2, 3$)
a_y	lateral acceleration, g units
a'_y	compensated lateral acceleration $\left(a_y - Y_{\delta_r}\delta_r\right)$, g units
b	wing span, m (ft)
$\Delta C_{D,ge}$	incremental drag coefficient due to ground effect
$\Delta C_{L,ge}$	incremental lift coefficient due to ground effect
$C_{l,1}, C_{l,2}$	rolling-moment coefficients
$\Delta C_{l,E1}$	incremental rolling-moment coefficient due to failure of engine 1

C_m pitching-moment coefficient

$C_{m,o}$ basic pitching-moment coefficient

$C_{m,1}, C_{m,2}$ pitching-moment coefficients

$C_{m,ge}$ incremental pitching-moment coefficient due to ground effect

$C_{n,1}, C_{n,2}$ yawing-moment coefficients

$\Delta C_{n,E1}$ incremental yawing-moment coefficient due to failure of engine 1

C_T thrust coefficient

C_X longitudinal-force coefficient

$C_{X,o}$ basic longitudinal-force coefficient

$C_{X,E1}$ incremental longitudinal force coefficient due to failure of engine 1

$C_{X,ge}$ longitudinal-force coefficient due to ground effects

$C_{Y,1}, C_{Y,2}$ side-force coefficients

$\Delta C_{Y,E1}$ incremental side-force coefficient due to failure of engine 1

C_Z vertical-force coefficient

$C_{Z,o}$ basic vertical-force coefficient

$C_{Z,E1}$ vertical-force coefficient with only three engines operating

$C_{Z,ge}$ vertical-force coefficient due to ground effects

$\bar{c}$ mean aerodynamic chord, m (ft)

f_1,f_2,f_3	forward, middle, and rearward segments, respectively, of the wing flaps
g	acceleration due to gravity, m/sec^2 (ft/sec^2)
h	altitude, m (ft)
I_X,I_Y,I_Z	moments of inertia about X_B, Y_B, and Z_B body axes, respectively, kg-m^2 (slug-ft^2)
I_{XZ}	product of inertia, kg-m^2 (slug-ft^2)
K	gain
m	mass of aircraft
p,q,r	rolling, pitching, and yawing angular velocities, respectively, deg/sec or rad/sec
S	wing area, m^2 (ft^2)
s	Laplace operator
T	thrust, N (lbf)
T_c	thrust commanded, N (lbf)
u,v,w	components of V in the X_B, Y_B, and Z_B directions, respectively
u_A,v_A,w_A	components of V_A in the X_B, Y_B, and Z_B directions, respectively
u_g,v_g,w_g	random gust velocity along the X_B, Y_B, and Z_B body axes, respectively, m/sec (ft/sec)
u'_g,v'_g,w'_g	random gust velocity along X_I, Y_I, and Z_I inertial axes, respectively, m/sec (ft/sec)
V	ground speed, knots (ft/sec)
V_A	resultant aerodynamic velocity of airplane, knots (ft/sec)

V_c velocity commanded, knots (ft/sec)

X distance from runway threshold, positive down runway, m (ft)

X', Y', Z' model displacement drive commands to RDS

X_B, Y_B, Z_B body coordinate axes fixed at airplane center of gravity

X_I, Y_I, Z_I inertial coordinate axes fixed at center of runway threshold

Y lateral displacement from localizer, m (ft)

$(\Delta Y)_{EO}$ maximum lateral displacement from localizer during recovery after engine-out condition, m (ft)

$$Y_{\delta_r} = \frac{\rho V_A^2 S C_{Y_{\delta_r}}}{2m}$$

α angle of attack, deg

β angle of sideslip, deg

δ_a aileron deflection, positive for right roll command, deg

δ_c control-column deflection, positive for pull force, deg

δ_{f1} deflection of forward segment of trailing-edge flap, deg

δ_{f2} deflection of second segment of trailing-edge flap, deg

δ_{f3} total deflection of rearward segment of trailing-edge flap, deg

δ^*_{f3} deflection of δ_{f3} from 60^o, deg $\left(\delta^*_{f3} = \delta_{f3} - 60^o\right)$

δ_{LT} cockpit controller for longitudinal trim

δ_p pedal travel, cm (in.)

δ_{RT} cockpit controller for roll trim

δ_r rudder deflection, deg

δ_s asymmetric deflection of spoilers for roll control, positive for right roll command, deg

$\delta_{s,int}$ asymmetric spoiler deflection beyond which ailerons are slaved to deflect with asymmetric spoiler, deg

δ_{sp} symmetrical deflection of spoilers for lift control, deg

δ_t horizontal-tail deflection, positive when trailing edge is deflected down, deg

δ_{th} throttle deflection, in.

δ_w control wheel deflection, deg

$(\epsilon_h)_{EO}$ altitude loss with respect to glide-slope beam following an engine-out condition, m (ft)

ϵ_y localizer error, deg

ϵ_z glide-slope error, deg

ϵ_{zh} glide-slope error, m (ft)

θ pitch angle, deg

θ' pitch model angle command or pitch command to RDS

ρ air density, kg/m^3 ($slugs/ft^3$)

τ time constant, sec

ϕ angle of roll, deg

ϕ' roll model angle command or roll command to RDS

ψ angle of heading, deg

ψ' yaw model angle command to RDS

$\Delta\psi$ heading error, deg

$[\ ]$ denotes matrix

$[\ ]^{-1}$ denotes inverse matrix

$$C_{l_\beta} = \frac{\partial C_l}{\partial \beta} \qquad C_{n_\beta} = \frac{\partial C_n}{\partial \beta} \qquad C_{Y_\beta} = \frac{\partial C_Y}{\partial \beta}$$

$$C_{X_{\delta^*_{f3}}} = \frac{\partial C_X}{\partial \delta^*_{f3}} \qquad C_{Z_{\delta^*_{f3}}} = \frac{\partial C_Z}{\partial \delta^*_{f3}} \qquad C_{m_{\delta^*_{f3}}} = \frac{\partial C_m}{\partial \delta^*_{f3}}$$

$$C_{X_{\delta_s}} = \frac{\partial C_X}{\partial \delta_s} \qquad C_{Z_{\delta_s}} = \frac{\partial C_Z}{\partial \delta_s} \qquad C_{m_{\delta_s}} = \frac{\partial C_m}{\partial \delta_s}$$

$$C_{l_{\delta_s}} = \frac{\partial C_l}{\partial \delta_s} \qquad C_{n_{\delta_s}} = \frac{\partial C_n}{\partial \delta_s} \qquad C_{Y_{\delta_s}} = \frac{\partial C_Y}{\partial \delta_s}$$

$$C_{X_{\delta_{sp}}} = \frac{\partial C_X}{\partial \delta_{sp}} \qquad C_{Z_{\delta_{sp}}} = \frac{\partial C_Z}{\partial \delta_{sp}} \qquad C_{m_{\delta_{sp}}} = \frac{\partial C_m}{\partial \delta_{sp}}$$

$$C_{X_{\delta_t}} = \frac{\partial C_X}{\partial \delta_t} \qquad C_{Z_{\delta_t}} = \frac{\partial C_Z}{\partial \delta_t} \qquad C_{m_{\delta_t}} = \frac{\partial C_m}{\partial \delta_t}$$

$$C_{l_{\delta_r}} = \frac{\partial C_l}{\partial \delta_r} \qquad C_{n_{\delta_r}} = \frac{\partial C_n}{\partial \delta_r} \qquad C_{Y_{\delta_r}} = \frac{\partial C_Y}{\partial \delta_r}$$

$$C_{l_{\delta_a}} = \frac{\partial C_l}{\partial \delta_a} \qquad C_{n_{\delta_a}} = \frac{\partial C_n}{\partial \delta_a} \qquad C_{Y_{\delta_a}} = \frac{\partial C_Y}{\partial \delta_a}$$

$$C_{l_p} = \frac{\partial C_l}{\partial \frac{pb}{2V}} \qquad C_{n_p} = \frac{\partial C_n}{\partial \frac{pb}{2V}} \qquad C_{Y_p} = \frac{\partial C_Y}{\partial \frac{pb}{2V}}$$

$$C_{l_r} = \frac{\partial C_l}{\partial \frac{rb}{2V}} \qquad C_{n_r} = \frac{\partial C_n}{\partial \frac{rb}{2V}} \qquad C_{Y_r} = \frac{\partial C_Y}{\partial \frac{rb}{2V}}$$

$$C_{m_q} = \frac{\partial C_m}{\partial \frac{q\bar{c}}{2V}} \qquad C_{m_{\dot{\alpha}}} = \frac{\partial C_m}{\partial \frac{\dot{\alpha}\bar{c}}{2V}} \qquad C_{L_\alpha} = \frac{\partial C_L}{\partial \alpha}$$

Abbreviations:

DLC	direct lift control
EO	engine out
EBF	externally blown flap
IFR	instrument flight rules
PIO	pilot-induced oscillations
RDS	real-time dynamic simulator
SAS	stability augmentation systems
STOL	short take-off and landing
VFR	visual flight rules

DESCRIPTION OF SIMULATED AIRCRAFT

The high-wing, T-tail STOL aircraft simulated in this study is essentially the same as the one used in the reference 4 study. A three-view drawing of the aircraft is shown in figure 1 along with assumed full-scale mass and dimensional characteristics. Control-surface deflections and maximum deflection rates are given in table I. Nondimensional aerodynamic characteristics for this aircraft were obtained from the wind-tunnel data curves of references 2 and 3. (See table II.) Also listed in table II are the coefficients (determined from the data curves of ref. 5), representing the so-called "negative ground effects." These ground effects are somewhat less severe than those used in the reference 4 study because they apply to a lower range of C_L values.

Four commercial high-bypass-turbofan engines which generate a combined maximum thrust of 147 058 N (33 060 lbf) were simulated. The engine characteristics are shown in table III. The engines were mounted to the underside of the wings and canted so that the exhaust impinged directly onto the trailing-edge flap system (see fig. 2) which was deployed for landing. The inboard engines were located at 0.22 semispan and the outboard pair at 0.42 semispan; this arrangement corresponds to the "spread-engine configuration" of references 2 and 4. The "clustered" engine configuration (outboard engines moved in to 0.30 semispan) of these references was also used during a few of the test approaches. This configuration is shown by the dashed lines in figure 1.

The wing incorporated blown (engine-bleed) leading-edge flaps (which were deflected 60°) and full-span, triple-slotted trailing-edge flaps (which were set at $\delta_{f1}/\delta_{f2}/\delta_{f3} = 25°/10°/60°$ for the approach and landing condition). A sketch of the flap assembly is shown in figure 2. The first two chordwise elements, f_1 and f_2, remained fixed at 25° and 10°, respectively, but the third chordwise element f_3 was implemented for active control (operating about the $\delta_{f3} = 60°$ reference position). An automatic speed control function was achieved by deflecting all six f_3 elements (three on each wing) symmetrically. Either the inboard or the middle f_3 elements on each wing were also deflected differentially for aileron roll control. Top-wing spoilers (fig. 2) were geared to the ailerons to produce additional roll control.

Two schemes were used for roll control, one for the clustered-engine configuration and the other for spread engines. The first scheme was to use the spoilers for primary control and gear the inboard f_3 elements as ailerons to assist when the spoilers reached ±30°. This scheme was used with clustered engines in the reference 4 study and again during the present study. The second scheme (for the spread-engine configuration) was to use the middle f_3 elements as ailerons for primary roll control and gear the spoilers to assist whenever the ailerons reached their travel limits of ±20°. This scheme is illustrated in figure 3 for a typical case of roll control during a landing approach where

the outboard engine on the right wing was failed (at approximately 19 sec). Prior to the engine failure, the ailerons were more than adequate for roll control, but when the failure occurred, they were driven at their maximum rate to their 20° limits. (The $\delta_a = -20°$ in fig. 3 corresponds to left-wing $\delta_{f3} = (60° - 20°)$ and right-wing $\delta_{f3} = (60° + 20°)$.) With the ailerons saturated, the left-wing spoilers were deflected an average of about 15° to overcome the remaining unbalanced rolling moment due to the failed engine. Continued roll control by the pilot was accomplished with the spoilers only because the ailerons remained saturated until touchdown.

The rudder on the vertical tail could be deflected ±40° for directional control. Leading-edge blowing on the rudder surface was used to increase rudder effectiveness at low speed. (See ref. 2.) The elevators were fixed at 50° (trailing edge up) for primary pitch trim of the high-lift landing configuration, and the entire horizontal tail (stabilator) was servodriven from the column or pitch-trim controller to achieve pitch control.

STABILITY AND COMMAND AUGMENTATION SYSTEMS

The STOL airplane used in this study was simulated with three different high-gain control systems (selected from ref. 4) having various degrees of stability and command augmentation. These aircraft-control configurations are designated herein as (1) BASIC, (2) BASIC + SAS, and (3) FULLY AUGMENTED. The same throttle gains and engine response characteristics (table III) were used for all configurations. Automatic speed control (AUTOSPEED) as depicted in figure 4 was also used with all configurations. The first two configurations involved the airplane with "clustered" engines only whereas the FULLY AUGMENTED airplane was simulated with only the spread-engine locations. The aerodynamic difference of the airplane for these two engine locations is indicated in part (b) of table II. As mentioned previously, the rearward segments of the inboard flaps were used as ailerons on the clustered-engine configuration whereas the rearward segments of the middle spanwise flaps were used as ailerons on the spread-engine configuration.

The control system for the BASIC airplane had no stability augmentation. This system is depicted in block diagram form in figure 5. The column, wheel, and pedals were position-command input devices for the horizontal tail, asymmetric spoilers plus ailerons, and rudder, respectively. All servoactuators were assumed to have first-order lags with 0.1-second time constants.

The control system for the BASIC + SAS configuration included a "basic" stability augmentation system (SAS) in addition to the AUTOSPEED. The SAS consisted of longitudinal augmentation as indicated in figure 6 and lateral-directional augmentation as indicated in figure 7. Generation of the $\dot{\beta}$ and a_y feedback signals is described in reference 4. It is recognized that the $\dot{\beta}$ signal is not readily available on most real airplanes

but with a modest onboard computational capability it can be generated. The important feature of the a_y' feedback is that it consists of both an outer loop a_y and an inner loop Y_{δ_r}. By using the gains specified in reference 4, the overall transfer function of the rudder servo became $\frac{10}{s + 23.2}$, whereas all other servos were modeled with $\frac{10}{s + 10}$.

The control system for the FULLY AUGMENTED airplane included longitudinal and lateral command augmentation. The longitudinal command augmentation is shown in the top half of figure 8. This system provided well-damped responses to pilot inputs with the column or pitch trim button and inherent pitch attitude stability (that is, "pitch hold") when no pilot inputs were made. The lateral command augmentation is shown in the bottom half of figure 8. This system (or control mode) is described as "roll-rate wheel steering" and provides a slightly stable spiral mode rather than "roll-hold" upon removal of a wheel command. Zero roll rate is commanded whenever there is no wheel input; thus, the system inherently acts to control (reduce) large rolling moments due to the failure of an engine. Thus, the task of recovery from an engine failure is made easier for the pilot because he does not have to react instantly to preclude a large lateral transient.

The pitch-attitude command system (fig. 8(a)) in effect replaces the longitudinal augmentation of figure 6 and the roll-rate command system (fig. 8(b)) replaces the lateral augmentation (that is, the part leading into the "aileron servo") depicted in figure 7. The directional SAS (or upper part of fig. 7) is then incorporated to complete the control system model for the FULLY AUGMENTED airplane.

DESCRIPTION OF SIMULATION EQUIPMENT

A block diagram of the moving-base RDS/STOL simulation system is given in figure 9. Real-time digital simulation techniques were used wherein the digital computer accepted inputs from the pilot's controls and made outputs to the simulation hardware 32 times each second. As indicated in the diagram, the outputs went to (1) the cockpit instruments, (2) a six-degree-of-freedom servodriven TV camera viewing a scale model of a STOL airport, (3) a remote abstract flight-director display, and (4) an analog computer which was used to generate special drive signals for the RDS motion system. A discussion of this special drive circuitry is presented in appendix A.

The RDS part of the simulation system was a large six-degree-of-freedom test bed located inside an aircraft hangar at Langley Research Center. Figure 10 is a photograph of this hardware. An example of the simulator response is shown in figure 11 which is an amplitude-phase plot of the response in the lateral degree of freedom. The relationships shown in this figure were typical of the simulator response in the other axes. A

general description of the RDS is given in reference 6 and a tabulation of its motion capabilities, both normal and as modified for this study, appears in appendix A.

Figure 12 is a photograph of the simulator instrument display and cockpit controls used in this study. The primary instrument 7 in the display group is the attitude indicator combined with a flight director. A conventional cross-pointer type of director (see appendix B) was used but the command bars were driven by signals and logic from the main computer program. A block-diagram indication of the flight-director drive signals is given in figure 13. The transfer functions were developed and the gains were optimized during the reference 4 study. In the present study only gains K_{22} and K_{23} were changed from the reference 4 value. Figure 14 is a photograph of the cockpit displays and includes the virtual image presentation of the airport scene and the heads-up flight-director display. The airport scene is controlled by the same computer as the airplane and thus "grows" realistically as the aircraft approaches the runway. Further discussion of the RDS/STOL cockpit, cockpit instruments, and heads-up flight-director display is given in appendix B.

As indicated in the Introduction, the same equations of motion, control systems, aircraft dynamics, and simulated atmospheric conditions as used for reference 4 were used in the present study. A summary of the equations is presented in appendix C.

RESULTS AND DISCUSSION

Two types of results are presented herein: (1) pilot evaluation of the handling qualities of an externally blown flap STOL aircraft while recovering from an "engine-out" (EO) during landing approach and (2) trajectory errors due to the EO. The approaches began from level flight (trimmed for the high-lift configuration) at an altitude of 243.8 m (800 ft) and about 3048 m (10 000 ft) from the runway threshold. A lateral offset of 121.9 m (400 ft) from the localizer was also used. The 6° glide slope was intercepted about 2320 m (7612 ft) from the threshold. The pilots were instructed to maintain the glide slope by holding a fixed vehicle pitch attitude and varying the flight path by increasing or decreasing thrust. Either the left or right outboard engine was failed at some altitude between 38.1 to 152.4 m (125 to 500 ft) during the approach. (The pilot was usually not warned in advance and a number of "non EO" approaches were randomly mixed in.) The pilots were not given the option to go around.

Time histories of several of the lateral-directional variables are shown in figure 15 for an Instrument Flight Rules (IFR) approach in turbulence with the FULLY AUGMENTED airplane. (The Y-trace is off-scale for the first 17 seconds because of the previously mentioned initial lateral offset.) The outboard engine on the left wing was failed at approximately 60 seconds. The reaction of the SAS was immediate and caused

the ailerons to satuate (δ_a-trace) and the spoiler on the right wing to activate. The pilot quickly superimposed a large control wheel (δ_w) input which drove the spoilers to a large angle and reversed the rolling moment. This reversal was quick enough to cause the spoiler to deactivate and the ailerons to come off their stops. Three smaller reverse $-\delta_w$ inputs were then made to stabilize the roll attitude and limit the transient lateral travel to less than 9 m (30 ft). The ailerons resumed their saturated position and the spoiler operated around a deflection level of about 10° to 15° until touchdown. Note that the return overshoot of the localizer (Y-trace) was about as large as the EO transient displacement, but the pilot reacquired the localizer and simultaneously brought the roll angle to zero in sufficient time to make a good center-of-the-runway landing.

Three aircraft-control configurations were flown with and without motion during the EO studies. A virtual-image TV scene of the airport was used during approaches under simulated visual flight rules (VFR). Automatic speed control (AUTOSPEED) and a flight director were used and were considered to be valuable aids for achieving good control and maintaining the pilot workload at an acceptable level during both VFR and IFR landing approaches. These aids were particularly important (and necessary) when command-control augmentation was not used.

EO Recovery During IFR Approaches

A summary of the pilot ratings of the handling qualities during IFR recovery attempts under several simulated conditions for each of the three configurations is given in table IV. The Cooper-Harper rating scale was used and is shown in table V. The ratings reflect the following:

(1) Only the FULLY AUGMENTED airplane handled satisfactorily under all approach conditions considered. It handled about as well in an EO situation as during a normal 6° glide-slope approach (in both the motion and nonmotion runs). The reason was that the augmentation precluded development of large upsetting moments which could lead to pilot-induced oscillations (PIO).

(2) The other two configurations handled poorly any time the lateral axis was upset. For example, with the BASIC airplane the failure of an engine and/or the presence of turbulence usually led to serious PIO situations, some of which would have been catastrophic in real life. The PIO situations were sometimes aggravated by the motion of the cockpit particularly when PIO conditions occurred in the pitch and roll axes simultaneously. Further investigation determined that the motion was valid for initial accelerations due to a disturbance on the aircraft; but if several sizable oscillations occurred, the phasing between the angular and linear accelerations became unrealistic and the pilots experienced difficulty in determining what their control response to the combined cue should be. The phasing problem was attributed in part to the different response

characteristics of the RDS linear and angular drive systems. Consequently, the unaugmented (that is, BASIC configuration) was removed from further consideration, partly because of its extremely poor lateral-directional handling qualities, but primarily because the RDS was found to be inadequate to accommodate some of its required motions because of a lateral upset.

(3) All three pilots said that it was easier to make the simulated EO recoveries in a nonmotion environment, but they all agreed that the motion environment felt more realistic (subject to the preceding PIO discussion) and typical of the conditions they would expect in a real situation. They said that the initial cockpit motion following an engine failure provided a helpful cue and alerted them to initiate a recovery action quickly. One pilot also commented that the simulator motion enhanced the turbulence simulation (which had seemed to be unreal during the fixed-base runs). Nevertheless, in a motion—no-motion comparison (see table IV), they rated the piloting tasks about equal for the FULLY AUGMENTED aircraft and favored the no-motion situation by about one rating point for the BASIC + SAS configuration.

In general, the pilots were not bothered by the failure of an outboard engine during approach with the FULLY AUGMENTED airplane because very little motion was involved. Because of the high-gain attitude stabilization, the pilots had to train themselves to remain out of the control loop until discrete inputs were definitely required. Even then, relatively small wheel and throttle inputs were sufficient and the pilots had to guard constantly against overresponding to an unexpected engine failure.

Everything was not back to a normal landing situation after recovery from an engine failure, however, because only a marginal amount of thrust was left for the flare and landing. Thus, there was an increased need to reach the flare point with favorable velocity components and aircraft attitude and to initiate the flare maneuver promptly. In order to accomplish this, the pilots preferred to concentrate strongly on their instruments during this phase and they tried to ignore all motion cues. The pilots commented that such a technique was not unusual because they also tended to ignore motion cues during the final phase of the landing approach with many airplanes in the real world.

Statistical results of the trajectory dispersions during 40 EO recoveries made with the FULLY AUGMENTED airplane under IFR conditions are shown in table VI. The measures of EO recovery are: (1) maximum altitude loss $(\epsilon_h)_{EO}$ with respect to the glide-slope beam and (2) maximum lateral deviation $(\Delta Y)_{EO}$ from the localizer during the transient motion. The point of touchdown (X and Y components with respect to the runway threshold and the center line, respectively) and the rate of sink $\dot{h}$ at flare initiation and at touchdown are also given in table VI. The $\dot{h}$ at flare initiation is included to indicate how well the pilot was able to restabilize the aircraft along the 6^{o} glide slope

following an EO. (Nominal $\dot{h}$ on the 6° glide slope is 4 m/sec (13.23 ft/sec) for the 75-knot approach speed.)

The results in smooth air were slightly better for the fixed-base set of runs than for the moving-base runs. The average maximum excursions and the standard deviations for recovery are smaller and the $\dot{h}$ at flare initiation is closer to nominal with a noticeably smaller standard deviation. The touchdown results are also better for the fixed-base runs. The X-values for the designated landing zone are 76 m to 213 m (250 ft to 700 ft).

The results of the 10 recoveries and touchdowns with motion and turbulence were the poorest of the three sets, although good control was maintained. (See fig. 15.) The engine failure was detected about as quickly as in smooth air and recovery action was prompt; however, precise reestablishment on the localizer and glide slope was not quickly achieved and the pilots were often still working on small error corrections when it came time for the flare. The pilots initiated the flares at the proper altitude but lift variations due to appreciable spoiler activity to control roll oscillations during the flare often resulted in relatively hard (mean $\dot{h}$ = 2.21 m/sec (7.25 ft/sec)) touchdowns. The associated standard deviations were also high because of the turbulence and because there were more roll corrections during the flare in some landings than in others.

An obvious modification to the flare maneuver for three-engine landings in turbulence is to initiate the flare at a slightly higher altitude than when all four engines are operational. To illustrate the technique, flares were initiated about 1.52 m (5 ft) higher than the nominal 16.15 m (53 ft) in several additional EO tests. Touchdowns occurred near the end of the landing zone at vertical velocities from 0.95 to 1.75 m/sec (3.08 to 5.76 ft/sec). Thus, it appeared that ideally this STOL could be landed with three engines in moderate turbulence about as well as with four engines in the same turbulence, but the control situation was potentially more critical because of the thrust limitation. Unlike four-engine flares where a thrust program was followed, the procedure for three-engine flares was inherently simplified in that maximum thrust (with three engines) was coincidentally the approximate amount required for flaring, provided $\dot{h}$ was near its nominal value at the flare-initiation altitude. Thus, the pilot usually commanded full throttles to command maximum powered lift (for the three operating engines) at the flare point and then waited for the touchdown. He had little time or capability to alter the flare trajectory along the way (unless pitch-command inputs were also made with the column).

EO Recovery During VFR Approaches

Landing approaches were made with the FULLY AUGMENTED configuration under simulated VFR conditions. When an engine was failed, the subsequent recovery was often less hurried than for IFR conditions because the pilot was visually assured that he was

maintaining adequate control of the airplane during the EO transient and recovery. Furthermore, with the airport in sight, he had an instinctive feel for the magnitude of the recovery action required and the time available to realine the airplane with the runway. Consequently, the maximum excursions away from the localizer and glide slope were somewhat greater than those for IFR approaches, but the recoveries were no less successful.

The pilots said that the difficulty of the piloting task during EO recovery was not significantly changed when the visual scene was added and used. The pilots further stated that the cues from the visual scene were realistic during the early approach, EO transients, and recovery because the gross altitude cues contained in the television picture were adequate for performing the control tasks. However, they were highly critical of the televised scene as the aircraft neared the runway (below 30 m (100 ft)). They said that during the flare maneuver they were not able to obtain the altitude and altitude-rate cues necessary for making good landings. (This deficiency had been noted in previous studies involving TV displays.) A large digital display of altitude was then superimposed on the landing scene, but it was generally ignored; the pilots did not particularly need this type of information above an altitude of 30 m (100 ft) and below 30 m they did not have time to monitor it effectively as they set up for and executed the flare.

When a simple "heads-up" flight-director display (see fig. 14) was superimposed on the landing scene and used by the pilots, they made the recoveries more quickly. The pilots commented that any slight improvement in recovery time could be attributed to their detection of the engine failure a fraction of a second sooner because of the initial visual and motion cues. They further stated that after detection they concentrated almost entirely on the heads-up flight director display until the recovery was nearly complete; then, they started to seek and use other visual references such as the runway. (No determination was made as to the value, if any, of visual cues obtained from the underlying landing scene while concentrating on the heads-up director.)

The VFR part of the study was terminated after it was demonstrated that no unexpected control problems were encountered during EO recoveries with the FULLY AUGMENTED aircraft and that there was no trend toward improved handling qualities because of the presence of the motion and visual cues.

CONCLUDING REMARKS

A moving-base simulation program has been conducted to study the problem of recovery and direct landing of an externally blown flap STOL aircraft after failure of an outboard engine during the final approach. The study results indicate the following:

1. Rather sophisticated stability and control augmentation systems are required to assist the pilot in maintaining precise control of this type of airplane after failure of an outboard engine. Considerable augmentation will also be required for normal four-engine approaches and landings.

2. The simulator motion and visual cues, in general, contributed realism to the simulation but did not effect the anticipated decrease in difficulty of the piloting task and/or reduction in stability augmentation system (SAS) complexity.

3. As the degree of control augmentation is reduced, serious pilot-induced oscillations (PIO) could result from lateral upsets because of strong turbulence or the failure of an engine. For such aircraft disturbances the initial motions of the simulator enhanced the control situation, but if a PIO tendency arose, then the phasing between the linear and angular cues degraded the motion cues. This condition, in turn, aggravated the PIO tendency and caused a degradation in overall control performance. The phasing problem was attributed to the inability to compensate adequately for inherent lag characteristics of the simulator in strong oscillatory situations.

4. The ratings assigned to the piloting task by the pilots during IFR approaches were not changed when a visual landing scene and/or a heads-up flight director were added to the simulation.

5. The piloting techniques and EO recovery results were about the same whether the pilots used the aircraft's regular flight director exclusively or the visual display which included the simple heads-up flight director. However, when the heads-up director was not included in the out-the-window display, the engine out (EO) recoveries were performed more slowly and maximum trajectory errors were larger, but the recoveries were equally successful.

6. With FULL AUGMENTATION and a reasonable amount of piloting compensation, the subject STOL aircraft could be landed satisfactorily in moderate turbulence with only three engines operating, but the control situation was potentially critical. Because of the thrust limitation, the important requisite for a good three-engine landing in turbulence was being able to restabilize the aircraft precisely on the glide slope before flare initiation and then promptly adding full thrust (for three engines) at the selected flare altitude. Inititation of the flare slightly above the selected flare altitude would be desirable if runway length were not critical.

Langley Research Center
National Aeronautics and Space Administration
Hampton, Va. 23665
July 2, 1975.

APPENDIX A

REAL-TIME DYNAMIC SIMULATOR (RDS)

The Langley real-time dynamic simulator (RDS) is a moving base simulator with independent motion drives in each of its six degrees of freedom. It consists of a simulator cockpit mounted in a three-axis gimbal system which is attached to a horseshoe-shaped support frame, which, in turn, is suspended by eight cables from an overhead carriage-dolly system. (See fig. 10.) The cables are arranged in a manner such that they provide nonpendulous suspension of the cockpit for horizontal accelerations less than 0.25g. The gimbals provide the three rotational degrees of freedom: the inner gimbal axis providing roll; the middle gimbal axis, yaw; and the outer gimbal axis, pitch. The three translational degrees of freedom are obtained through the carriage-dolly system. Vertical motion is achieved by rotating a large drum which winds up the eight cables attached to the gimbal support frame. The cable drum is mounted on the dolly which rides on tracks mounted across the main carriage. The main carriage moves along another pair of rails (see fig. 10) attached under the roof of an aircraft hangar at Langley Research Center. The simulator cockpit for the present study was oriented as shown in figure 10. The landing approach was assumed to be in a direction approximately normal to the direction of the main carriage motion. This arrangement permitted use of the large operating envelope of the main carriage for the potentially large lateral motions associated with failure of an outboard engine.

The basic RDS drive systems are capable of the following maximum displacements, velocities, and accelerations:

RDS motion drive performance			
Cockpit axis	Maximum displacement	Maximum velocity	Maximum acceleration
Lateral	±22.86 m (±75 ft)	±2.44 m/sec (±8 ft/sec)	±2.44 m/sec^2 (±8 ft/sec^2)
Longitudinal	±2.44 m (±8 ft)	±1.22 m/sec (±4 ft/sec)	±1.22 m/sec^2 (±4 ft/sec^2)
Vertical	±6.1 m (±20 ft)	±1.83 m/sec (±6 ft/sec)	±1.83 m/sec^2 (±6 ft/sec^2)
Pitch	± Continuous rotation	±1 rad/sec	±1 rad/sec^2
Yaw	± Continuous rotation	±1 rad/sec	±1 rad/sec^2
Roll	± Continuous rotation	±1 rad/sec	±1 rad/sec^2

However, the motion was restricted to the following values for the present study:

Restricted motion drive performance			
Cockpit axis	Maximum displacement	Maximum velocity	Maximum acceleration
Lateral	±22.86 m (±75 ft)	±2.13 m/sec (±7 ft/sec)	±2.44 m/sec^2 (±8 ft/sec^2)
Longitudinal	0.0 (0.0)	0.0 (0.0)	0.0 (0.0)
Vertical	±6.1 m (±20 ft)	±1.83 m/sec (±6 ft/sec)	±1.83 m/sec^2 (±6 ft/sec^2)
Pitch	±0.7 rad	±1 rad/sec	±1 rad/sec^2
Yaw	±0.35 rad	±1 rad/sec	±1 rad/sec^2
Roll	±0.35 rad	±1 rad/sec	±1 rad/sec^2

The vertical and lateral motion drives were not restricted, but the longitudinal axis motion drive was deactivated completely because significant longitudinal accelerations were not expected. The restricted angular motion was dictated by the size and shape of the STOL cockpit. The use of these restricted motion envelopes, however, did not interfere with the motion requirements for the present study.

The RDS drive components in each axis are, by necessity, large and fairly complex. Hence, system response is dramatically affected by the interaction of the various mechanical subsystems comprising the total drive system. Therefore, during the initial design and construction of the RDS facility, internal electronic circuitry was used to minimize these interactions and to optimize the system response over a fairly large frequency range. Hence, when operating in a restricted motion envelope, the drive signals can be tuned for best response in the restricted region by preconditioning those signals. To accomplish this for the present study, an analog computer was inserted between the digital-computer model and the RDS. (See fig. 9.) The analog computer was used to manipulate the drive signals to obtain the best dynamic response of the RDS, with respect to the model, for the frequency range required for the present study. A combination of several motion drive techniques including "motion scaling," "washout," "feed forward," and "motion onset" were used. The resultant computer-generated motion-drive signals reproduced motion cues, within the capability of the simulator, that were most nearly representative of those produced by the simulated STOL aircraft. The following computer schematic diagrams show the circuitry used to manipulate the drive signals for each axis. Below each diagram is its associated transfer function in Laplace transform representation.

APPENDIX A

Lateral and vertical:

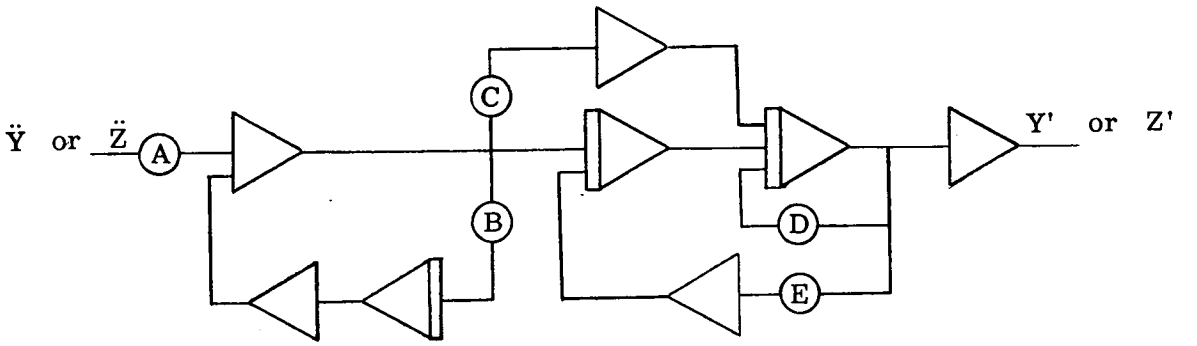

$$\frac{Y'}{\ddot{Y}} = \frac{A(Cs^2 + s)}{(s + B)(s^2 + Ds + E)}$$

Pitch and roll:

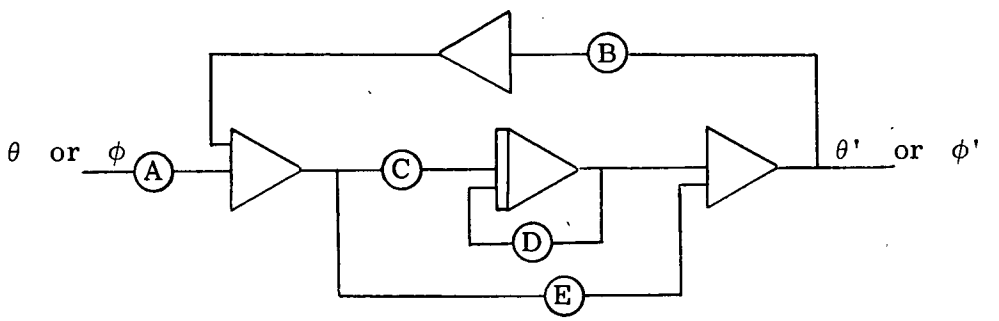

$$\frac{\theta'}{\theta} = \frac{A[E(s + D) - C]}{(1 + EB)(s + D) - CB}$$

Yaw:

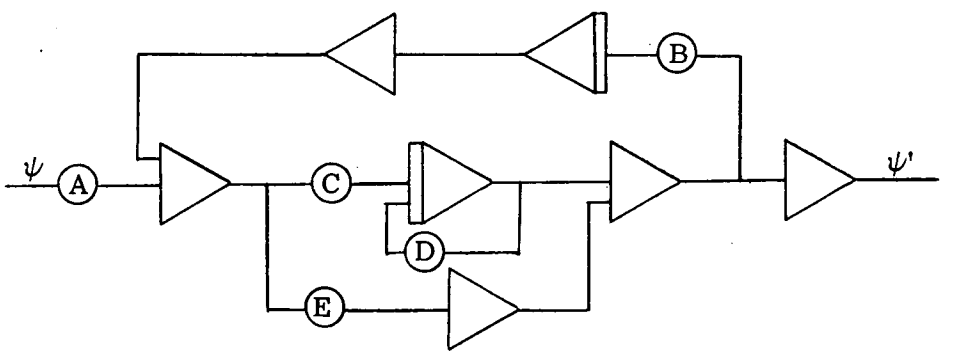

$$\frac{\psi'}{\psi} = \frac{A\left[Es^2 + (ED + C)s\right]}{s^2 + (D + BE)s + B(C + ED)}$$

APPENDIX A

In addition to manipulating the drive signals based on prior theoretical analysis, once the circuitry was developed, experienced NASA research pilots tuned the final system by performing various maneuvers with the simulated aircraft and had the perceived acceleration levels (and other angular cues) adjusted to match the dynamics of the computed aircraft as indicated by the cockpit instruments.

As is explained in the body of the report, the motion drive was only partly successful. Good correspondence was obtained for most motions, but, on occasion, when an exaggerated PIO tendency occurred, the induced motion would degrade rather than enhance the simulation.

APPENDIX B

THE SIMULATOR COCKPIT AND VISUAL DISPLAY

The cockpit which was installed on the Langley real-time dynamic simulator (RDS) for the STOL landing approach simulation was essentially the left half of a side-by-side four-engine transport airplane cockpit. The interior of the cockpit (attitude controls, instrument package, and various cockpit items) was arranged similar to the fixed-base simulator cockpit used in the reference 4 study.

A pilot's view of the instrument panel and the flight control components is illustrated in figure 12. Only the components identified by number were used in the present simulation. The primary instrument monitored was the "flight director" (designated 7).

A close-up view of the flight director is given in figure 16. The components of the flight director pertinent to the STOL simulation fall into three basic groups: attitude, situation, and command. The attitude group consisted of the horizon line, pitch- and roll-attitude sphere, miniature airplane symbol, and roll-attitude pointer. The situation group consisted of a glide-slope pointer, localizer pointer, and the radio altitude bar. The command group consisted of a pair of flight-director bars driven by a signal composed of the elements and shaping indicated in figure 13. Acquisition of and staying on the glide slope and localizer were accomplished by manipulating the appropriate vehicle controls so that the flight director bars were kept centered on the dot in the middle of the miniature airplane symbol. The preferred procedure for acquiring and maintaining the glide slope during a landing approach was to hold a fixed-vehicle pitch attitude and vary the flight path by increasing or decreasing thrust. The horizontal situation indicator (HSI) located directly below the flight director provided heading information and duplicated the localizer information presented on the flight director.

The various lights and switches are identified in figure 12. The three lights located over the altimeter and numbered 9, 10, and 11 were used to indicate warning and initiation cues to the pilot during the simulated landing flare and touchdown. The vertically arranged pair of lights (designated 16) were used to indicate to the pilot the proper trim position for the throttles (designated 18) prior to initiating a test approach. Individual instrument illumination was provided by installing post lights at the airspeed, altimeter, rate-of-climb, angle-of-attack, and direct lift control (DLC) instruments.

The switches located on the control wheel were as follows: On the left horn of the wheel a button (designated 1) was used to engage the autospeed control. Usually the pilot activated the autospeed circuit with this switch immediately after beginning a test approach. The thumb switch (designated 2) on the left control horn was a four-way aircraft trim switch for pilot-initiated changes in vehicle pitch and roll trim. The DLC

thumb wheel (designated 14) on the right horn was an optional method for making small changes in thrust. This option was generally ignored in lieu of the throttle.

The control column and wheel dimensions are shown in the following sketch. The control motion dampers were set for a control damping ratio of 0.7. They were disconnected during the system force-deflection calibrations.

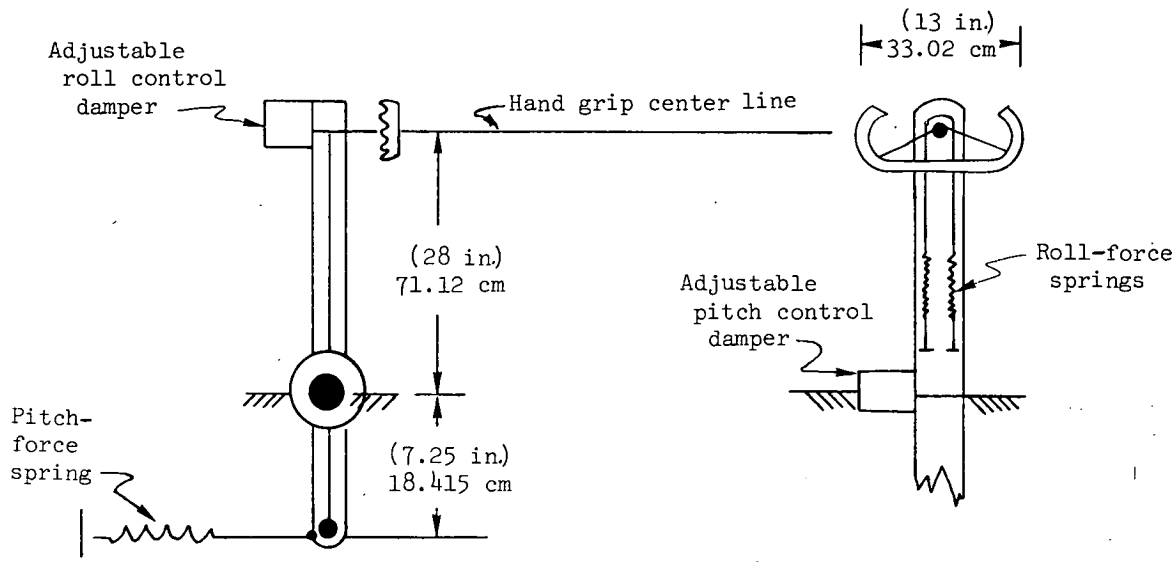

A force-deflection diagram for pitch control is shown in figure 17. A similar diagram for roll control is shown in figure 18. The control forces chosen were a composite of forces from military specifications (ref. 7), pilot opinion (NASA test pilots), and various aircraft of similar configuration and performance. (For example, see ref. 8.) A roll-control force gradient of 0.4 lb/deg was chosen (that is, 0.2 lb/deg/hand). The pitch-control force gradient for these tests was 14.23 N/deg (3.2 lb/deg).

Rudder pedals were installed in the cockpit. For the FULLY AUGMENTED airplane rudder pedal inputs were not required. The pilots did use the rudder pedals when the degree of augmentation was reduced.

For VFR approaches, a virtual image scene of a typical STOL airport was presented to the pilot. The airport scene was obtained by using the computed aircraft motions to drive a six-degree-of-freedom color TV camera system over a 1/300-scale model of a simulated STOL airport. This scene was transmitted to the simulator cockpit by closed circuit TV and displayed on a 63.50-cm (25-in.) color TV monitor which was mounted on a bracket forward of the windshield. The pilot viewed the scene on the monitor through a virtual image lens which represented the windshield. (See fig. 14.)

Thrust-command information for glide-slope tracking and roll-command information for localizer tracking were combined into a heads-up flight director display located

appropriately in the windshield field of view. This display consisted of two fixed parallel bars and a moving dot which appeared to be focused at infinity rather than on the windshield itself. A typical location used during the study is shown in figure 14. The dot was usually zeroed halfway between the right-hand ends of the parallel bars (as shown in fig. 14). One pilot preferred a single-line display with the dot zeroed at the midpoint of the line.

The bar-dot display was generated on a cathode-ray tube (CRT) and viewed by a second TV camera. The video signal from this camera was then mixed with the video signal from the camera viewing the airport scene. The combined signal was transmitted to the 63.50-cm (25-in.) monitor at the simulator cockpit.

APPENDIX C

SIMULATION EQUATIONS

The aircraft equations of motion and related equations are presented in this appendix. The forces and moments acting on the aircraft are summed in a conventional body-axis system X_B, Y_B, Z_B with origin at the center of gravity of the aircraft. The gravity force and wind conditions are defined in an Earth-fixed or inertial axis system X_I, Y_I, Z_I and transformed into the body system.

The linear acceleration components in the X_B, Y_B, and Z_B directions, respectively, are given by

$$\begin{bmatrix} \dot{u} \\ \dot{v} \\ \dot{w} \end{bmatrix} = \begin{bmatrix} -g \sin\theta + vr - wq + \frac{\rho V_A{}^2 S}{2m} C_X \\ g \cos\theta \sin\phi + wp - ur + \frac{\rho V_A{}^2 S}{2m} C_{Y,1} + \frac{\rho V_A S b}{4m} C_{Y,2} \\ g \cos\theta \cos\phi + uq - vp + \frac{\rho V_A{}^2 S}{2m} C_Z \end{bmatrix} \tag{1}$$

$$C_X = C_{X,o} + C_{X_{\delta_t}} \delta t + C_{X_{\delta_{f3}^*}} \delta_{f3}^* + C_{X_{\delta_{sp}}} \delta sp + C_{X_{\delta_s}} |\delta s| + C_{X,ge} + C_{X,E1} \tag{2}$$

$$C_{Y,1} = C_{Y_\beta} \beta + C_{Y_{\delta_r}} \delta r + C_{Y_{\delta_a}} \delta a + C_{Y_{\delta_s}} \delta s + \Delta C_{Y,E1} \tag{3}$$

$$C_{Y,2} = C_{Y_p} p + C_{Y_r} r \tag{4}$$

$$C_Z = C_{Z,o} + C_{Z_{\delta_t}} \delta t + C_{Z_{\delta_{f3}^*}} \delta_{f3}^* + C_{Z_{\delta_{sp}}} \delta sp + C_{Z_{\delta_s}} |\delta s| + C_{Z,ge} + C_{Z,E1} \tag{5}$$

where

$$C_Y = C_{Y,1} + C_{Y,2}$$

The coefficients on the right are, in turn, defined analytically in the section "Symbols" and numerically by the values in table II. The spoiler deflections (see fig. 2) are always upward but the asymmetric-spoiler deflection angle δ_S is defined in terms of

the rolling moment it induces; thus, δ_s appears as an absolute value in equations (2) and (5) but not in equation (3) because the sense of the Y force is dependent on the sign of δ_s. Coefficients with the subscript "E1" are used with appropriate logic to introduce the effects of failing either outboard engine.

The angular acceleration components are given by

$$\begin{bmatrix} \dot{p} \\ \dot{q} \\ \dot{r} \end{bmatrix} = \begin{bmatrix} \frac{I_Y - I_Z}{I_X} qr + \frac{I_{XZ}}{I_X}(\dot{r} + pq) + \frac{\rho V_A{}^2 Sb}{2I_X} C_{l,1} + \frac{\rho V_A Sb^2}{4I_X} C_{l,2} \\ \frac{I_Z - I_X}{I_Y} pr + \frac{I_{XZ}}{I_Y}(r^2 - p^2) + \frac{\rho V_A{}^2 S\bar{c}}{2I_Y} C_{m,1} + \frac{\rho V_A S\bar{c}^2}{4I_Y} C_{m,2} \\ \frac{I_X - I_Y}{I_Z} pq + \frac{I_{XZ}}{I_Z}(\dot{p} - qr) + \frac{\rho V_A{}^2 Sb}{2I_Z} C_{n,1} + \frac{\rho V_A Sb^2}{4I_Z} C_{n,2} \end{bmatrix} \tag{6}$$

where I_X, I_Y, and I_Z are moments of inertia about the body axes of the aircraft and I_{XZ} is the associated product of inertia. The nondimensional moment coefficients on the right of equation (6) are defined by

$$C_{l,1} = C_{l_\beta}\beta + C_{l_{\delta_r}}\delta r + C_{l_{\delta_a}}\delta a + C_{l_{\delta_s}}\delta s + \Delta C_{l,E1} \tag{7}$$

$$C_{l,2} = C_{l_p}p + C_{l_r}r \tag{8}$$

$$C_{m,1} = C_{m,o} + C_{m_{\delta_t}}\delta t + C_{m_{\delta^*_{f3}}}\delta^*_{f3} + C_{m_{\delta_{sp}}}\delta sp + C_{m_{\delta_s}}|\delta s| + C_{m,ge} \tag{9}$$

$$C_{m,2} = C_{m_q}q + C_{m_{\dot{\alpha}}}\dot{\alpha} \tag{10}$$

$$C_{n,1} = C_{n_\beta}\beta + C_{n_{\delta_r}}\delta r + C_{n_{\delta_a}}\delta a + C_{n_{\delta_s}}\delta s + \Delta C_{n,E1} \tag{11}$$

$$C_{n,2} = C_{n_p}p + C_{n_r}r \tag{12}$$

where

$$C_l = C_{l,1} + C_{l,2}$$

$$C_m = C_{m,1} + C_{m,2}$$

$$C_n = C_{n,1} + C_{n,2}$$

Specific values of the coefficients on the right-hand sides of equations (2) to (5) and (7) to (12) were determined from table II by means of a "table-lookup" interpolation scheme in the computer program.

The wind conditions used in the simulation were included as follows. The total aerodynamic velocity of the aircraft is given by

$$V_A = \left(u_A^2 + v_A^2 + w_A^2\right)^{1/2} \tag{13}$$

where

$$\begin{bmatrix} u_A \\ v_A \\ w_A \end{bmatrix} = \begin{bmatrix} u + u_g \\ v + v_g \\ w + w_g \end{bmatrix} \tag{14}$$

The components u_g, v_g, and w_g are transformed wind velocities given by

$$\begin{bmatrix} u_g \\ v_g \\ w_g \end{bmatrix} = \begin{bmatrix} \quad \\ a_{ij} \\ \quad \end{bmatrix} \begin{bmatrix} u'_g \\ v'_g \\ w'_g \end{bmatrix} \qquad (i = 1, 2, 3; \quad j = 1, 2, 3) \tag{15}$$

where u'_g, v'_g, and w'_g are defined in the Earth-fixed axis system as constants or as functions of altitude. The direction-cosine elements of the transformation matrix $[a_{ij}]$ are

$$a_{11} = \cos\theta \cos\psi \tag{16}$$

$$a_{12} = \cos\theta \sin\psi \tag{17}$$

$$a_{13} = -\sin\theta \tag{18}$$

$$a_{21} = \sin\phi \cos\psi \sin\theta - \cos\phi \sin\psi \tag{19}$$

$$a_{22} = \sin\phi \sin\psi \sin\theta + \cos\phi \cos\psi \tag{20}$$

$$a_{23} = \sin\phi \cos\theta \tag{21}$$

$$a_{31} = \cos\phi \cos\psi \sin\theta + \sin\phi \sin\psi \tag{22}$$

$$a_{32} = \cos\phi \sin\psi \sin\theta - \sin\phi \cos\psi \tag{23}$$

$$a_{33} = \cos\phi \cos\theta \tag{24}$$

The Euler angles ψ, θ, and ϕ are derived from

$$\left.\begin{aligned} \dot{\psi} &= \frac{r\cos\phi + q\sin\phi}{\cos\theta} \\ \dot{\theta} &= q\cos\phi - r\sin\phi \\ \dot{\phi} &= p + \dot{\psi}\sin\theta \end{aligned}\right\} \tag{25}$$

In addition to the wind conditions just discussed, random turbulence could be superimposed on the velocity components in each axis. The turbulence model is based on the Dryden spectral form and involves feeding Gaussian white noise from three independent random number generators through shaping filters. The filter transfer functions are presented and discussed in reference 4. Rotational gusts were not simulated.

The origin of the inertial axes X_I, Y_I, and Z_I was located at the runway threshold, with X_I pointing down the runway center line and Y_I to the right. Altitude h is calculated as $-Z_I$. Equations for the inertial displacements are determined from

$$\begin{bmatrix} \dot{X} \\ \dot{Y} \\ -\dot{h} \end{bmatrix} = \begin{bmatrix} \\ a_{ij} \\ \\ \end{bmatrix}^{-1} \begin{bmatrix} u \\ v \\ w \end{bmatrix} \qquad (i = 1, 2, 3; \quad j = 1, 2, 3) \qquad (26)$$

where $[a_{ij}]^{-1}$ is the inverse of the $[a_{ij}]$ used in equation (15). The glide slope was assumed to intersect the runway at $X = 76.2$ m (250 ft) and the localizer source was assumed to be at $X = 1219.2$ m (4000 ft). The landing zone was designated as $76 \leqq X \leqq 213$ m ($250 \leqq X \leqq 700$ ft). The angles ϵ_y and ϵ_z are aircraft position errors with respect to the localizer and glide slope, respectively. They are determined by

$$\epsilon_y = \tan^{-1} \frac{Y}{4000 - X} \qquad (27)$$

$$\epsilon_z = \tan^{-1} \frac{h - 12}{250 - X} - \text{Glide-slope angle} \qquad (28)$$

The instantaneous altitude h in the ϵ_z equation was biased 3.7 m (12 ft) because the landing gear of the simulated aircraft extends this distance below its center of gravity. (The variables X, Y, and h must be expressed in feet when used in equations (27) and (28).)

REFERENCES

1. Crane, Harold L.; Sommer, Robert W.; and Healy, Frederick M.: Effects of Reduced Airspeed for Landing Approach on Flying Qualities of a Large Jet Transport Equipped With Powered Lift. NASA TN D-4804, 1968.

2. Parlett, Lysle P.; Greer, H. Douglas; Henderson, Robert L.; and Carter, C. Robert: Wind-Tunnel Investigation of an External-Flow Jet-Flap Transport Configuration Having Full-Span Triple-Slotted Flaps. NASA TN D-6391, 1971.

3. Grafton, Sue B.; Parlett, Lysle P.; and Smith, Charles C., Jr.: Dynamic Stability Derivatives of a Jet Transport Configuration With High Thrust-Weight Ratio and an Externally Blown Jet Flap. NASA TN D-6440, 1971.

4. Grantham, William D.; Nguyen, Luat T.; Patton, James M., Jr.; Deal, Perry L.; Champine, Robert A.; and Carter, C. Robert: Fixed-Base Simulator Study of an Externally Blown Flap STOL Transport Airplane During Approach and Landing. NASA TN D-6898, 1972.

5. Vogler, Raymond D.: Wind-Tunnel Investigation of a Four-Engine Externally Blowing Jet-Flap STOL Airplane Model. NASA TN D-7034, 1970.

6. Connor, Andrew B.; Bergeron, Hugh P.; and Schoonover, W. Elliott, Jr.: Ride-Quality Research Activities at NASA Langley Research Center. Symposium on Vehicle Ride Quality, NASA TM X-2620, 1972, pp. 229-246.

7. Anon.: Flying Qualities of Piloted Airplanes. Mil. Specif. MIL-F-8785B(AG), Aug. 7, 1969.

8. Innis, Robert C.; Holzhauser, Curt A.; and Quigley, Hervey C.: Airworthiness Considerations for STOL Aircraft. NASA TN D-5594, 1970.

TABLE I.- RANGE OF CONTROL-SURFACE DEFLECTIONS AND MAXIMUM DEFLECTION RATES

Control surface	Range of deflection angle, deg	Maximum deflection rate, deg/sec
Horizontal tail	±10	50
Rear wing flap	0 to 90	5
Spoilers	0 to 60	50
Aileron	±20	50
Rudder	±40	50

TABLE II.- BASIC AERODYNAMIC INPUTS USED IN SIMULATION

$[\delta_{f3}^* = \delta_{f3} - 60]$

(a) Clustered engines

α, deg	C_T=0	C_T=1.87	C_T=3.74	C_T=0	C_T=1.87	C_T=3.74	C_T=0	C_T=1.87	C_T=3.74	C_T=0	C_T=1.87	C_T=3.74	C_T=0	C_T=1.87	C_T=3.74	C_T=0	C_T=1.87	C_T=3.74	C_T=0	C_T=1.87	C_T=3.74	C_T=0	C_T=1.87	C_T=3.74
	C_X			C_Z			C_m			$C_{X_{\delta_{f3}^*}}$, per deg			$C_{Z_{\delta_{f3}^*}}$, per deg			$C_{m_{\delta_{f3}^*}}$, per deg			C_{m_q}, per rad			$C_{m_{\dot{\alpha}}}$, per rad		
-10	-0.330	-0.211	0.383	-0.145	-3.212	-4.739	0.80	0.25	-0.50	-0.0038	-0.0460	-0.0760	-0.0180	-0.0550	-0.0400	-0.0001	0.0016	-0.0036	-28.60	-17.86	-28.60	-11.40	-7.14	-11.40
-5	-.366	-.232	.285	-.741	-3.794	-5.345	.45	.10	-.50	-.0033	-.0435	-.0736	-.0134	-.0580	-.0610	.0006	.0021	-.0023	-28.60	-26.80	-28.60	-11.40	-10.70	-11.40
0	-.340	-.250	.300	-1.400	-4.500	-6.130	.12	-.07	-.53	-.0026	-.0403	-.0700	-.0086	-.0611	-.0861	.0013	.0026	-.0010	-28.60	-32.15	-29.30	-11.40	-12.85	-11.70
5	-.249	-.119	.432	-2.090	-5.180	-6.889	-.14	-.25	-.60	-.0029	-.0388	-.0690	-.0089	-.0593	-.0832	.0019	.0022	0	-26.45	-34.30	-30.00	-10.55	-13.70	-12.00
10	-.094	.095	.594	-2.518	-5.781	-7.572	-.23	-.37	-.68	-.0040	-.0371	-.0674	-.0040	-.0534	-.0784	.0019	.0034	.0003	-21.44	-32.86	-30.36	-8.56	-13.14	-12.14
15	.017	.344	.932	-2.770	-6.306	-8.116	-.27	-.45	-.78	-.0041	-.0360	-.0649	.0009	-.0490	-.0759	.0033	.0030	.0005	-10.72	-30.72	-31.45	-4.28	-12.28	-12.55
20	.019	.632	1.162	-2.851	-6.708	-8.601	-.27	-.50	-.84	-.0051	-.0350	-.0627	.0054	-.0492	-.0737	.0026	.0020	-.0005	-3.57	-30.00	-31.45	-1.43	-12.00	-12.55
25	.078	.864	1.535	-2.700	-7.033	-8.972	-.30	-.49	-.83	-.0046	-.0320	-.0591	.0040	-.0455	-.0734	.0030	.0016	-.0004	-5.00	-28.60	-30.36	-2.00	-11.40	-12.14
30	.111	.798	1.765	-2.592	-5.602	-9.258	-.32	-.40	-.75	-.0055	-.0099	-.0514	.0060	-.0527	-.0683	.0022	.0042	-.0006	-9.29	-39.30	-48.60	-3.71	-15.70	-19.40
	$C_{X_{\delta_s}}$, per deg			$C_{Z_{\delta_s}}$, per deg			$C_{m_{\delta_s}}$, per deg			$C_{Y_{\delta_s}}$, per deg			$C_{n_{\delta_s}}$, per deg			$C_{l_{\delta_s}}$, per deg			C_{Y_p}, per rad			C_{n_p}, per rad		
-10	-0.0012	-0.0024	-0.0026	0.0093	0.0140	0.0148	-0.0012	0.0006	0.0052	-0.0002	0	0.0002	0.0007	0.0007	0.0005	0.0015	0.0023	0.0024	-0.02	-0.09	-0.49	-0.15	-0.11	0.38
-5	-.0016	-.0016	-.0028	.0105	.0165	.0161	-.0017	-.0007	.0025	-.0002	-.0001	.0002	.0008	.0008	.0009	.0020	.0029	.0028	-.04	-.04	-.10	-.04	-.15	-.12
0	-.0020	-.0008	-.0030	.0117	.0192	.0173	-.0022	-.0020	-.0002	-.0002	-.0002	0	.0009	.0009	.0013	.0025	.0035	.0032	0	.05	.11	-.02	-.22	-.30
5	-.0026	-.0013	-.0032	.0128	.0209	.0173	-.0008	-.0022	-.0017	-.0002	-.0002	-.0001	.0009	.0010	.0015	.0027	.0038	.0033	.07	.19	.10	-.20	-.28	-.25
10	-.0033	-.0021	-.0028	.0119	.0217	.0185	-.0002	-.0020	-.0020	-.0003	-.0003	-.0002	.0009	.0011	.0015	.0026	.0038	.0032	.05	.25	.53	-.16	-.33	-.40
15	-.0035	-.0033	-.0046	.0099	.0219	.0186	.0008	-.0012	-.0012	-.0002	-.0003	-.0002	.0009	.0011	.0015	.0022	.0036	.0031	.24	.45	.80	-.20	-.45	-.52
20	-.0028	-.0037	-.0033	.0078	.0210	.0176	.0013	-.0008	-.0005	-.0002	-.0003	-.0002	.0008	.0011	.0014	.0017	.0035	.0029	.30	.80	1.20	-.22	-.50	-.57
25	-.0017	-.0032	-.0048	.0036	.0209	.0163	.0017	-.0008	-.0002	-.0002	-.0004	-.0002	.0008	.0010	.0013	.0011	.0037	.0028	.06	.89	1.25	-.15	-.40	-.59
30	0	-.0068	-.0029	.0015	.0117	.0160	.0020	-.0012	-.0005	-.0002	-.0004	-.0003	.0007	.0010	.0012	.0008	.0038	.0028	.13	.75	1.03	-.14	-.22	-.15
	$C_{X_{\delta_t}}$, per deg			$C_{Z_{\delta_t}}$, per deg			$C_{m_{\delta_t}}$, per deg			$C_{Y_{\delta_r}}$, per deg			$C_{n_{\delta_r}}$, per deg			$C_{l_{\delta_r}}$, per deg			C_{l_p}, per rad			C_{Y_r}, per rad		
-10	-0.0092	0.0072	-0.0049	-0.0242	-0.0160	-0.0102	-0.090	-0.084	-0.028	0.012	0.010	0.009	-0.0043	-0.0051	-0.0046	0.0020	0.0016	0.0019	-0.05	-1.13	-0.78	0.76	0.88	0.94
-5	-.0062	.0042	-.0019	-.0246	-.0204	-.0101	-.085	-.087	-.044	.012	.010	.009	-.0041	-.0047	-.0046	.0018	.0016	.0020	-.60	-.88	-.75	.76	.86	.92
0	-.0030	.0010	.0010	-.0250	-.0250	-.0100	-.080	-.090	-.060	.012	.010	.009	-.0039	-.0043	-.0046	.0016	.0016	.0021	-.98	-.68	-.72	.77	.90	1.00
5	-.0002	-.0012	.0004	-.0201	-.0202	-.0050	-.065	-.097	-.076	.011	.010	.009	-.0038	-.0041	-.0046	.0016	.0017	.0022	-.68	-.50	-.68	.77	1.03	1.20
10	-.0036	-.0044	-.0070	-.0138	-.0211	-.0174	-.040	-.092	-.088	.010	.010	.009	-.0036	-.0040	-.0046	.0016	.0017	.0022	-.40	-.50	-.63	.78	1.08	1.60
15	-.0018	-.0071	-.0015	-.0088	-.0122	-.0252	-.013	-.078	-.098	.010	.010	.010	-.0034	-.0040	-.0046	.0011	.0017	.0022	-.37	-.50	-.55	.80	1.00	1.35
20	-.0006	-.0011	.0002	-.0042	-.0057	-.0180	.002	-.069	-.089	.009	.011	.010	-.0024	-.0040	-.0046	.0003	.0016	.0020	-.32	-.33	-.42	.59	.70	1.24
25	-.0042	-.0051	-.0030	-.0053	-.0079	-.0124	.002	-.060	-.080	.006	.012	.012	-.0020	-.0041	-.0047	-.0003	.0010	.0017	-.26	-.17	-.33	.33	.32	.93
30	-.0002	-.0152	.0339	-.0036	-.0312	-.0728	-.005	-.050	-.079	.002	.010	.012	-.0002	-.0033	-.0042	.0006	.0008	.0014	-.26	-.08	-.25	-.08	1.70	2.55
	C_{Y_β}, per deg			C_{n_β}, per deg			C_{l_β}, per deg			$C_{X_{\delta_{sp}}}$, per deg			$C_{Z_{\delta_{sp}}}$, per deg			$C_{m_{\delta_{sp}}}$, per deg			C_{n_r}, per rad			C_{l_r}, per rad		
-10	-0.020	-0.022	-0.050	0.0030	0.0035	0.0053	0.0012	0	0	0	-0.0060	-0.0044	0.0260	0.0430	0.0300	-0.006	0	0.008	-0.45	-0.33	-0.37	0.32	0.57	0.55
-5	-.020	-.050	-.050	.0038	.0052	.0070	-.0006	-.0020	-.0020	-.0016	-.0043	-.0042	.0272	.0425	.0325	-.004	0	.005	-.35	-.38	-.42	.48	.70	.77
0	-.020	-.050	-.055	.0042	.0078	.0081	-.0024	-.0036	-.0031	-.0040	-.0010	-.0040	.0290	.0420	.0380	-.002	0	.002	-.30	-.42	-.45	.67	.80	.86
5	-.020	-.050	-.055	.0043	.0082	.0086	-.0034	-.0048	-.0044	-.0048	-.0018	-.0056	.0317	.0440	.0417	0	0	.001	-.33	-.41	-.45	.77	.85	.85
10	-.020	-.050	-.055	.0043	.0080	.0081	-.0023	-.0051	-.0053	-.0052	-.0016	-.0045	.0296	.0434	.0429	.001	0	.001	-.34	-.42	-.54	.83	.80	.80
15	-.023	-.050	-.055	.0047	.0082	.0089	-.0028	-.0051	-.0061	-.0046	-.0012	-.0080	.0247	.0432	.0414	.004	.001	.002	-.38	-.42	-.52	.88	.82	.83
20	-.024	-.050	-.055	.0050	.0084	.0092	-.0029	-.0062	-.0066	-.0036	-.0046	-.0070	.0157	.0420	.0387	.005	.001	.002	-.35	-.40	-.52	.73	.90	.90
25	-.020	-.050	-.055	.0021	.0083	.0088	-.0070	-.0067	-.0072	.0001	-.0025	-.0085	.0045	.0408	.0347	.004	.001	.003	-.30	-.34	-.47	.83	1.10	.93
30	-.024	-.020	-.055	.0018	-.0040	.0082	-.0050	-.0070	-.0090	.0012	-.0082	-.0024	.0019	-.0022	.0321	.004	.001	.003	-.20	-.42	-.70	.62	-.20	-.50

TABLE II.- BASIC AERODYNAMIC INPUTS USED IN SIMULATION - Continued

(a) Clustered engines – Concluded

α, deg	C_T=0	C_T=0.70	C_T=1.40	C_T=2.10	C_T=2.81	C_T=0	C_T=0.70	C_T=1.40	C_T=2.10	C_T=2.81	C_T=0	C_T=0.70	C_T=1.40	C_T=2.10	C_T=2.81	C_T=0	C_T=0.70	C_T=1.40	C_T=2.10	C_T=2.81	C_T=0	C_T=0.70	C_T=1.40	C_T=2.10	C_T=2.81
	$\Delta C_{Y,E1}$					$\Delta C_{n,E1}$					$\Delta C_{l,E1}$					$C_{X,E1}$					$C_{Z,E1}$				
-10	0	0.009	0.011	0.005	0.005	0	-0.026	-0.032	-0.038	-0.059	-0.004	-0.030	-0.102	-0.118	-0.162	-0.42	-0.58	-0.62	-0.51	-0.40	-0.07	-1.86	-2.73	-3.28	-3.82
-5	0	.007	.008	.005	0	0	-.021	-.030	-.043	-.055	-.001	-.040	-.100	-.133	-.171	-.36	-.52	-.49	-.38	-.25	-.76	-2.45	-3.30	-3.94	-4.55
0	0	.005	.005	.005	-.005	0	-.016	-.028	-.048	-.051	.002	-.050	-.098	-.148	-.180	-.30	-.46	-.36	-.25	-.10	-1.45	-3.04	-3.87	-4.60	-5.28
5	0	.002	.002	.005	.001	0	-.014	-.023	-.045	-.048	0	-.064	-.104	-.160	-.195	-.20	-.28	-.22	-.14	-.01	-2.05	-3.68	-4.46	-5.35	-6.02
10	-.001	.006	.006	.007	.003	0	-.010	-.020	-.040	-.048	0	-.075	-.115	-.165	-.210	-.07	-.12	-.05	.10	.20	-2.46	-4.17	-5.08	-5.96	-6.55
15	.001	.008	.008	.010	.006	-.002	-.012	-.024	-.043	-.052	-.003	-.086	-.127	-.229	-.228	.03	.11	.18	.31	.42	-2.72	-4.55	-5.44	-6.20	-6.91
20	.004	.013	.024	.025	.015	.005	-.036	-.069	-.087	-.085	.002	-.186	-.355	-.367	-.365	.09	.31	.46	.62	.73	-2.73	-4.34	-5.39	-6.49	-7.38
25	.003	.012	.023	.026	.029	-.002	-.021	-.044	-.065	-.098	-.003	-.134	-.266	-.348	-.490	.09	.53	.88	1.20	1.12	-2.59	-4.04	-5.26	-6.59	-7.56
30	.004	.008	.010	.019	.021	0	.003	-.005	-.027	-.040	-.001	-.048	-.125	-.237	-.373	.12	.64	1.15	1.44	1.32	-2.51	-3.89	-5.06	-6.20	-6.76
	$C_{Y_{\delta_a}}$, per deg					$C_{n_{\delta_a}}$, per deg					$C_{l_{\delta_a}}$, per deg														
-10	-0.0016	-0.0010	-0.0004	0.0002	0.0008	-0.0014	-0.0028	-0.0040	-0.0052	-0.0064	0.0082	0.0083	0.0084	0.0085	0.0086										
-5	-.0012	-.0007	-.0002	.0003	.0008	-.0001	-.0017	-.0032	-.0047	-.0062	.0048	.0058	.0068	.0078	.0088										
0	-.0008	-.0004	0	.0004	.0008	.0012	-.0006	-.0024	-.0042	-.0060	.0014	.0033	.0052	.0071	.0090										
5	-.0004	-.0002	0	.0002	.0004	-.0010	-.0022	-.0034	-.0046	-.0058	.0014	.0033	.0052	.0071	.0090										
10	-.0006	-.0004	-.0002	0	.0002	-.0010	-.0022	-.0034	-.0046	-.0058	.0010	.0030	.0050	.0070	.0090										
15	-.0008	-.0006	-.0004	-.0002	.0001	.0004	-.0011	-.0026	-.0041	-.0056	.0027	.0044	.0061	.0078	.0096										
20	-.0022	-.0018	-.0014	-.0010	-.0005	.0045	.0026	.0007	-.0012	-.0032	.0207	.0197	.0187	.0177	.0168										
25	-.0036	-.0024	-.0012	0	-.0012	.0036	.0024	.0010	-.0002	-.0014	-.0010	.0050	.0110	.0170	.0240										
30	-.0007	-.0006	-.0005	-.0004	-.0003	.0024	.0008	-.0008	-.0024	-.0040	-.0076	-.0012	.0052	.0116	.0180										

TABLE II.- BASIC AERODYNAMIC INPUTS USED IN SIMULATION - Continued

(b) Spread engines. (Inputs same as for clustered engines except for coefficients herein.)

α, deg	C_T=0	C_T=1.40	C_T=2.81	C_T=0	C_T=1.40	C_T=2.81	C_T=0	C_T=1.40	C_T=2.81
	$\Delta C_{Y,E1}$			$\Delta C_{n,E1}$			$\Delta C_{\ell,E1}$		
-10	-0.010	0.065	-0.017	-0.002	-0.040	-0.060	-0.042	-0.135	-0.190
-5	0	.045	-.029	-.002	-.040	-.069	-.020	-.130	-.192
0	-.005	.032	-.035	-.003	-.038	-.073	-.003	-.129	-.200
5	0	.048	.003	-.001	-.041	-.083	.002	-.146	-.223
10	0	.055	.025	-.001	-.038	-.088	0	-.161	-.251
15	0	.050	.037	-.001	-.044	-.095	.002	-.185	-.278
20	.015	.070	.125	-.002	-.049	-.102	.002	-.178	-.318
25	.015	.185	.225	0	-.061	-.114	.002	-.253	-.392
30	.020	.075	.175	-.004	-.036	-.077	0	-.133	-.270
	$C_{Y_{\delta_a}}$, per deg			$C_{n_{\delta_a}}$, per deg			$C_{\ell_{\delta_a}}$, per deg		
-10	0.0005	-0.0058	-0.0042	0.0008	0.0002	-0.0010	0.0024	0.0038	0.0041
-5	-.0025	-.0022	-.0050	.0008	.0002	.0002	.0013	.0035	.0046
0	-.0032	-.0051	-.0068	.0009	.0002	.0008	.0003	.0034	.0049
5	-.0055	-.0074	-.0082	.0008	.0006	.0010	-.0001	.0038	.0056
10	-.0050	-.0078	-.0088	.0008	.0004	.0014	0	.0041	.0058
15	-.0050	-.0075	-.0094	.0010	.0006	.0018	.0020	.0052	.0068
20	-.0062	-.0085	-.0134	.0018	.0006	.0020	.0044	.0046	.0084
25	-.0062	-.0112	-.0182	.0018	.0019	.0021	.0045	.0116	.0120
30	-.0075	-.0068	-.0128	.0016	.0011	.0004	.0026	.0033	.0108

TABLE II.- BASIC AERODYNAMIC INPUTS USED IN SIMULATION – Concluded

(c) Ground effects (same for clustered and spread engines)

h		$C_L = 3.0$	$C_L = 3.5$	$C_L = 4.0$	$C_L = 3.0$	$C_L = 3.5$	$C_L = 4.0$	$C_L = 3.0$	$C_L = 3.5$	$C_L = 4.0$
m	ft	$\Delta C_{L,ge}$			$\Delta C_{D,ge}$			$\Delta C_{m,ge}$		
0	0	-0.090	-0.154	-0.239	-0.19	-0.24	-0.29	-0.15	-0.30	-0.48
3	10	-.020	-.050	-.095	-.08	-.11	-.14	-.08	-.15	-.23
6.1	20	-.008	-.026	-.050	0	0	0	0	0	0
9.1	30	-.002	-.005	-.009	0	0	0	0	0	0

$$C_{X,ge} = \Delta C_{L,ge} \sin \alpha - \Delta C_{D,ge} \cos \alpha$$

$$C_{Z,ge} = -\Delta C_{L,ge} \cos \alpha - \Delta C_{D,ge} \sin \alpha$$

TABLE III. - SIMULATED ENGINE RESPONSE CHARACTERISTICS

[The thrust values are presented in units of newtons (pounds force)]

(a) Acceleration

Time, sec	Thrust response for T_c, N (lbf), of –										
	2611 (587)	6530 (1468)	13 625 (3063)	16 796 (3776)	22 023 (4951)	36 764 (8265)	6904 (1552)	14 741 (3314)	18 847 (4237)	21 649 (4867)	36 764 (8265)
0	1681 (378)	1681 (378)	1 681 (378)	1 681 (378)	1 681 (378)	1 681 (378)	2611 (587)	2 611 (587)	2 611 (587)	2 611 (587)	2 611 (587)
.2	1681 (378)	1681 (378)	1 681 (378)	1 681 (378)	1 681 (378)	1 681 (378)	2705 (608)	2 705 (608)	2 705 (608)	2 705 (608)	2 705 (608)
.4	1775 (399)	1775 (399)	1 775 (399)	1 775 (399)	1 775 (399)	1 775 (399)	2798 (629)	2 798 (629)	2 798 (629)	2 798 (629)	2 798 (629)
.6	1868 (420)	1868 (420)	1 868 (420)	1 868 (420)	1 868 (420)	1 868 (420)	2985 (671)	2 985 (671)	2 985 (671)	2 985 (671)	2 985 (671)
.8	2055 (462)	2055 (462)	2 055 (462)	2 055 (462)	2 055 (462)	2 055 (462)	3358 (755)	3 358 (755)	3 358 (755)	3 358 (755)	3 358 (755)
1.0	2144 (482)	2144 (482)	2 144 (482)	2 144 (482)	2 144 (482)	2 144 (482)	4106 (923)	4 106 (923)	4 106 (923)	4 106 (923)	4 106 (923)
1.2	2331 (524)	2331 (524)	2 331 (524)	2 331 (524)	2 331 (524)	2 331 (524)	5227 (1175)	5 227 (1175)	5 227 (1175)	5 227 (1175)	5 227 (1175)
1.4	2424 (545)	2611 (587)	2 611 (587)	2 611 (587)	2 611 (587)	2 611 (587)	5600 (1259)	7 090 (1594)	7 277 (1636)	7 277 (1636)	7 277 (1636)
1.6	2518 (566)	2985 (671)	2 985 (671)	2 985 (671)	2 985 (671)	2 985 (671)	5880 (1322)	10 449 (2349)	10 449 (2349)	10 449 (2349)	10 449 (2349)
1.8	2611 (587)	3545 (797)	3 545 (797)	3 545 (797)	3 545 (797)	3 545 (797)	6161 (1385)	11 196 (2517)	12 691 (2853)	12 691 (2853)	15 302 (3440)
2.0		4012 (902)	4 386 (986)	4 386 (986)	4 386 (986)	4 386 (986)	6343 (1426)	11 943 (2685)	14 372 (3231)	15 115 (3398)	18 473 (4153)
2.2		4666 (1049)	5 600 (1259)	5 600 (1259)	5 600 (1259)	5 600 (1259)	6437 (1447)	12 504 (2811)	15 489 (3482)	16 796 (3776)	21 649 (4867)
2.4		5040 (1133)	8 211 (1846)	8 211 (1846)	8 211 (1846)	8 211 (1846)	6623 (1489)	12 878 (2895)	16 329 (3671)	17 917 (4028)	24 447 (5496)
2.6		5600 (1259)	9 519 (2140)	11 383 (2559)	11 383 (2559)	11 383 (2559)	6717 (1510)	13 158 (2958)	16 983 (3818)	18 571 (4175)	26 876 (6042)
2.8		5974 (1343)	10 360 (2329)	12 686 (2852)	15 395 (3461)	16 610 (3734)	6810 (1531)	13 438 (3021)	17 357 (3902)	19 034 (4279)	28 740 (6461)
3.0		6250 (1405)	11 196 (2517)	13 812 (3105)	16 983 (3818)	21 276 (4783)	6904 (1552)	13 625 (3063)	17 637 (3965)	19 407 (4363)	30 048 (6755)
3.2		6437 (1447)	11 943 (2685)	14 741 (3314)	18 104 (4070)	24 634 (5538)		13 718 (3084)	17 824 (4007)	19 781 (4447)	31 258 (7027)
3.4		6530 (1468)	12 317 (2769)	15 302 (3440)	18 571 (4175)	27 619 (6209)		13 905 (3126)	18 011 (4049)	19 968 (4489)	32 378 (7279)
3.6			12 691 (2853)	15 675 (3524)	19 034 (4279)	29 487 (6629)		13 998 (3147)	18 104 (4070)	20 248 (4552)	33 126 (7447)
3.8			12 878 (2895)	15 956 (3587)	19 407 (4363)	31 164 (7006)		14 092 (3168)	18 198 (4091)	20 417 (4590)	33 780 (7594)
4.0			13 251 (2979)	16 143 (3629)	19 781 (4447)	32 472 (7300)		14 185 (3189)	18 384 (4133)	20 715 (4657)	34 340 (7720)
4.2			13 438 (3021)	16 236 (3650)	20 061 (4510)	33 499 (7531)		14 279 (3210)	18 473 (4153)	20 809 (4678)	34 807 (7825)
4.4			13 625 (3063)	16 423 (3692)	20 342 (4573)	34 153 (7678)		14 372 (3231)	18 571 (4175)	20 996 (4720)	35 270 (7929)
4.6				16 516 (3713)	20 435 (4594)	34 714 (7804)		14 466 (3252)	18 665 (4196)	21 089 (4741)	35 643 (8013)
4.8				16 610 (3734)	20 622 (4636)	35 270 (7929)		14 555 (3272)	18 754 (4216)	21 182 (4762)	35 924 (8076)
5.0				16 703 (3755)	20 715 (4657)	35 643 (8013)		14 648 (3293)	18 847 (4237)	21 276 (4783)	36 204 (8139)
5.2				16 796 (3776)	20 902 (4699)	36 017 (8097)		14 741 (3314)		21 463 (4825)	36 391 (8181)
5.4					20 996 (4720)	36 297 (8160)				21 556 (4846)	36 578 (8223)
5.6					21 089 (4741)	36 578 (8223)				21 649 (4867)	36 671 (8244)
5.8					21 276 (4783)	36 671 (8244)					36 764 (8265)
6.0					21 463 (4825)	36 764 (8265)					
6.2					21 556 (4846)						
6.4					21 649 (4867)						
6.6					21 930 (4930)						
6.8					22 023 (4951)						

TABLE III. - SIMULATED ENGINE RESPONSE CHARACTERISTICS – Continued

[The thrust values are presented in units of newtons (pounds force)]

(a) Acceleration – Concluded

Time, sec	Thrust response for T_c, N (lbf), of –											
	36 764 (8265)	18 198 (4091)	36 764 (8265)	13 905 (3126)	22 397 (5035)	36 764 (8265)	19 594 (4405)	22 953 (5160)	36 764 (8265)	22 953 (5160)	36 764 (8265)	36 764 (8265)
0	4 479 (1007)	11 196 (2517)	11 196 (2517)	12 317 (2769)	12 317 (2769)	12 317 (2769)	16 796 (3776)	16 796 (3776)	16 796 (3776)	20 715 (4657)	20 715 (4657)	24 447 (5496)
.2	4 853 (1091)	12 317 (2769)	12 317 (2769)	12 878 (2895)	13 998 (3147)	13 998 (3147)	18 291 (4112)	19 221 (4321)	19 221 (4321)	21 836 (4909)	24 074 (5412)	27 806 (6251)
.4	5 600 (1259)	14 555 (3272)	15 675 (3524)	13 251 (2979)	16 796 (3776)	16 796 (3776)	18 940 (4258)	20 342 (4573)	24 074 (5412)	22 116 (4972)	30 048 (6755)	31 912 (7174)
.6	7 090 (1594)	15 302 (3440)	20 528 (4615)	13 438 (3021)	18 291 (4112)	22 397 (5035)	19 127 (4300)	21 089 (4741)	27 993 (6293)	22 303 (5014)	32 472 (7300)	33 407 (7510)
.8	9 519 (2140)	16 049 (3608)	24 634 (5538)	13 531 (3042)	19 407 (4363)	26 129 (5874)	19 407 (4363)	21 836 (4909)	30 608 (6881)	22 490 (5056)	33 780 (7594)	34 528 (7762)
1.0	12 878 (2895)	16 610 (3734)	27 993 (6293)	13 625 (3063)	20 342 (4573)	29 113 (6545)	19 594 (4405)	22 397 (5035)	32 472 (7300)	22 677 (5098)	34 527 (7762)	35 644 (8013)
1.2	17 917 (4028)	17 170 (3860)	30 234 (6797)	13 718 (3084)	20 902 (4699)	30 888 (6944)		22 677 (5098)	33 593 (7552)	22 770 (5119)	35 087 (7888)	36 205 (8139)
1.4	22 397 (5035)	17 357 (3902)	31 538 (7090)	13 812 (3105)	21 463 (4825)	32 285 (7258)		22 953 (5160)	34 247 (7699)	22 953 (5160)	35 643 (8013)	36 764 (8265)
1.6	25 755 (5790)	17 637 (3965)	32 472 (7300)	13 905 (3126)	21 930 (4930)	33 219 (7468)			34 714 (7804)		36 017 (8097)	
1.8	28 553 (6419)	17 917 (4028)	33 219 (7468)		22 210 (4993)	33 966 (7636)			35 270 (7929)		36 391 (8181)	
2.0	30 421 (6839)	18 011 (4049)	33 780 (7594)		22 397 (5035)	34 527 (7762)			35 830 (8055)		36 764 (8265)	
2.2	31 444 (7069)	18 104 (4070)	34 340 (7720)			35 087 (7888)			36 204 (8139)			
2.4	32 285 (7258)	18 198 (4091)	34 714 (7804)			35 457 (7971)			36 578 (8223)			
2.6	32 846 (7384)		35 270 (7929)			35 830 (8055)			36 764 (8265)			
2.8	33 499 (7531)		35 830 (8055)			36 297 (8160)						
3.0	34 153 (7678)		36 204 (8139)			36 578 (8223)						
3.2	34 714 (7804)		36 484 (8202)			36 764 (8265)						
3.4	35 087 (7888)		36 671 (8244)									
3.6	35 457 (7971)		36 764 (8265)									
3.8	35 737 (8034)											
4.0	35 924 (8076)											
4.2	36 110 (8118)											
4.4	36 204 (8139)											
4.6	36 391 (8181)											
4.8	36 484 (8202)											
5.0	36 578 (8223)											
5.2	36 671 (8244)											
5.4	36 764 (8265)											

TABLE III.- SIMULATED ENGINE RESPONSE CHARACTERISTICS – Continued

[The thrust values are presented in units of newtons (pounds force)]

(b) Deceleration

Time, sec	Thrust response for T_c, N (lbf), of –									
	1 681 (378)	8 772 (1972)	17 357 (3902)	19 781 (4447)	24 447 (5496)	1 681 (378)	13 069 (2938)	16 796 (3776)	21 836 (4909)	1 681 (378)
0	36 764 (8265)	36 764 (8265)	36 764 (8265)	36 764 (8265)	36 764 (8265)	24 634 (5538)	24 634 (5538)	24 634 (5538)	23 513 (5286)	22 770 (5119)
.2	32 846 (7384)	32 846 (7384)	32 846 (7384)	32 846 (7384)	32 846 (7384)	21 743 (4888)	21 743 (4888)	22 210 (4993)	23 046 (5181)	20 155 (4531)
.4	26 876 (6042)	26 876 (6042)	26 876 (6042)	26 876 (6042)	26 876 (6042)	19 221 (4321)	19 221 (4321)	20 155 (4531)	22 677 (5098)	18 198 (4091)
.6	22 397 (5035)	22 397 (5035)	24 447 (5496)	24 634 (5538)	24 634 (5538)	17 170 (3860)	17 170 (3860)	19 034 (4279)	22 397 (5035)	16 049 (3608)
.8	18 847 (4237)	18 847 (4237)	22 584 (5077)	23 700 (5328)	24 447 (5496)	15 675 (3524)	15 675 (3524)	18 478 (4154)	22 210 (4993)	13 998 (3147)
1.0	16 610 (3734)	16 610 (3734)	21 463 (4825)	23 140 (5202)		14 092 (3168)	15 022 (3377)	18 104 (4070)	22 116 (4972)	12 504 (2811)
1.2	14 928 (3356)	15 302 (3440)	21 099 (4741)	22 770 (5119)		12 691 (2853)	14 555 (3272)	17 824 (4007)	21 930 (4930)	11 290 (2538)
1.4	13 812 (3105)	14 372 (3231)	20 715 (4657)	22 397 (5035)		11 196 (2517)	14 092 (3168)	17 637 (3965)	21 836 (4909)	10 449 (2349)
1.6	12 504 (2811)	13 812 (3105)	20 342 (4573)	22 210 (4993)		10 449 (2349)	13 812 (3105)	17 450 (3923)		9 706 (2182)
1.8	11 570 (2601)	13 438 (3021)	19 968 (4489)	22 023 (4951)		9 519 (2140)	13 438 (3021)	17 357 (3902)		8 959 (2014)
2.0	10 916 (2454)	12 971 (2916)	19 594 (4405)	21 836 (4909)		8 772 (1972)	13 251 (2979)	17 263 (3881)		8 398 (1888)
2.2	10 266 (2308)	12 691 (2853)	19 221 (4321)	21 649 (4867)		8 211 (1846)	13 069 (2938)	17 170 (3860)		7 838 (1762)
2.4	9 519 (2140)	12 410 (2790)	19 034 (4279)	21 463 (4825)		7 838 (1762)		17 077 (3839)		7 277 (1636)
2.6	8 772 (1972)	12 130 (2727)	18 847 (4237)	21 276 (4783)		7 371 (1657)		16 983 (3818)		6 904 (1552)
2.8	8 211 (1846)	11 943 (2685)	18 665 (4196)	21 089 (4741)		6 997 (1573)		16 890 (3797)		6 530 (1468)
3.0	7 838 (1762)	11 663 (2622)	18 478 (4154)	20 902 (4699)		6 717 (1510)		16 796 (3776)		6 161 (1385)
3.2	7 464 (1678)	11 476 (2580)	18 291 (4112)	20 809 (4678)		6 343 (1426)				5 787 (1301)
3.4	7 090 (1594)	11 290 (2538)	18 198 (4091)	20 715 (4657)		5 974 (1343)				5 600 (1259)
3.6	6 717 (1510)	11 103 (2496)	18 104 (4070)	20 528 (4615)		5 600 (1259)				5 320 (1196)
3.8	6 530 (1468)	11 009 (2475)	18 011 (4049)	20 435 (4594)		5 413 (1217)				5 133 (1154)
4.0	6 161 (1385)	10 822 (2433)	17 917 (4028)	20 342 (4573)		5 227 (1175)				4 853 (1091)
4.2	5 974 (1343)	10 636 (2391)	17 824 (4007)	20 248 (4552)		5 040 (1133)				4 573 (1028)
4.4	5 694 (1280)	10 449 (2349)	17 731 (3986)	20 155 (4531)		4 760 (1070)				4 386 (986)
4.6	5 413 (1217)	10 360 (2329)	17 637 (3965)	20 061 (4510)		4 479 (1007)				4 106 (923)
4.8	5 227 (1175)	10 266 (2308)	17 544 (3944)	19 968 (4489)		4 293 (965)				3 825 (860)
5.0	5 040 (1133)	10 080 (2266)	17 450 (3923)	19 875 (4468)		4 107 (923)				3 639 (818)
5.2	4 853 (1091)	9 986 (2245)	17 357 (3902)	19 781 (4447)		3 732 (839)				3 452 (776)
5.4	4 479 (1007)	9 893 (2224)				3 545 (797)				3 265 (734)
5.6	4 293 (965)	9 706 (2182)				3 358 (755)				3 172 (713)
5.8	4 106 (923)	9 613 (2161)				3 265 (734)				2 985 (671)
6.0	3 919 (881)	9 519 (2140)				3 078 (692)				2 798 (629)
6.2	3 732 (839)	9 426 (2119)				2 985 (671)				2 705 (608)
6.4	3 545 (797)	9 239 (2077)				2 798 (629)				2 518 (566)
6.6	3 172 (713)	9 145 (2056)				2 611 (587)				2 424 (545)
6.8	2 985 (671)	9 052 (2035)				2 424 (545)				2 237 (503)
7.0	2 798 (629)	8 959 (2014)				2 237 (503)				2 055 (462)
7.2	2 611 (587)	8 865 (1993)				2 055 (462)				1 962 (441)
7.4	2 424 (545)	8 772 (1972)				1 868 (420)				1 868 (420)
7.6	2 144 (482)					1 681 (378)				1 775 (399)
7.8	1 868 (420)									1 681 (378)
8.0	1 681 (378)									

TABLE III. - SIMULATED ENGINE RESPONSE CHARACTERISTICS – Concluded

[The thrust values are presented in units of newtons (pounds force)]

(b) Deceleration – Concluded

Time, sec	Thrust response for T_c, N (lbf), of –									
	3 732 (839)	17 917 (4028)	11 917 (2679)	1 681 (378)	7 464 (1678)	3 732 (839)	12 691 (2853)	1 681 (378)	3732 (839)	1681 (378)
0	20 155 (4531)	20 155 (4531)	18 754 (4216)	17 824 (4007)	17 824 (4007)	15 115 (3398)	13 998 (3147)	13 438 (3021)	7464 (1678)	5413 (1217)
.2	18 847 (4237)	19 034 (4279)	17 450 (3923)	16 423 (3692)	16 049 (3608)	14 372 (3231)	13 625 (3063)	12 504 (2811)	7184 (1615)	5133 (1154)
.4	17 170 (3860)	18 665 (4196)	15 862 (3566)	14 555 (3272)	14 741 (3314)	13 438 (3021)	13 345 (3000)	11 570 (2601)	6810 (1531)	4853 (1091)
.6	15 302 (3440)	18 478 (4154)	14 555 (3272)	13 158 (2958)	13 812 (3105)	12 130 (2727)	13 158 (2958)	10 636 (2391)	6437 (1447)	4573 (1028)
.8	13 438 (3021)	18 291 (4112)	13 812 (3105)	11 757 (2643)	12 878 (2895)	10 822 (2433)	12 971 (2916)	9 706 (2182)	6067 (1364)	4293 (965)
1.0	11 943 (2685)	18 104 (4070)	13 345 (3000)	10 449 (2349)	11 943 (2685)	9 706 (2182)	12 913 (2903)	8 772 (1972)	5694 (1280)	4012 (902)
1.2	10 822 (2433)	17 917 (4028)	12 971 (2916)	9 332 (2098)	11 383 (2559)	8 959 (2014)	12 878 (2895)	8 025 (1804)	5320 (1196)	3732 (839)
1.4	9 893 (2224)		12 691 (2853)	8 398 (1888)	10 822 (2433)	8 211 (1846)	12 784 (2874)	7 277 (1636)	5040 (1133)	3545 (797)
1.6	9 145 (2056)		12 504 (2811)	7 838 (1762)	10 449 (2349)	7 464 (1678)	12 726 (2861)	6 717 (1510)	4760 (1070)	3358 (755)
1.8	8 492 (1909)		12 410 (2790)	7 090 (1594)	10 080 (2266)	6 904 (1552)	12 691 (2853)	6 161 (1385)	4573 (1028)	3078 (692)
2.0	7 838 (1762)		11 917 (2679)	6 530 (1468)	9 706 (2182)	6 437 (1447)		5 787 (1301)	4293 (965)	2891 (650)
2.2	7 277 (1636)			6 067 (1364)	9 332 (2098)	5 974 (1343)		5 413 (1217)	4199 (944)	2611 (587)
2.4	6 904 (1552)			5 600 (1259)	9 145 (2056)	5 600 (1259)		5 040 (1133)	4106 (923)	2424 (545)
2.6	6 530 (1468)			5 227 (1175)	8 865 (1993)	5 413 (1217)		4 666 (1049)	4012 (902)	2237 (503)
2.8	6 161 (1385)			4 853 (1091)	8 585 (1930)	5 040 (1133)		4 293 (965)	3919 (881)	2144 (482)
3.0	5 787 (1301)			4 479 (1007)	8 398 (1888)	4 760 (1070)		4 012 (902)	3825 (860)	1962 (441)
3.2	5 413 (1217)			4 293 (965)	8 118 (1825)	4 479 (1007)		3 732 (839)	3732 (839)	1868 (420)
3.4	5 133 (1154)			3 919 (881)	7 838 (1762)	4 293 (965)		3 452 (776)		1775 (399)
3.6	4 853 (1091)			3 732 (839)	7 650 (1720)	4 106 (923)		3 172 (713)		1681 (378)
3.8	4 666 (1049)			3 545 (797)	7 557 (1699)	3 919 (881)		2 985 (671)		
4.0	4 386 (986)			3 265 (734)	7 464 (1678)	3 732 (839)		2 798 (629)		
4.2	4 106 (923)			2 985 (671)				2 611 (587)		
4.4	3 919 (881)			2 798 (629)				2 424 (545)		
4.6	3 732 (839)			2 611 (587)				2 237 (503)		
4.8				2 518 (566)				2 055 (462)		
5.0				2 331 (524)				1 868 (420)		
5.2				2 237 (503)				1 775 (399)		
5.4				2 055 (462)				1 681 (378)		
5.6				1 868 (420)						
5.8				1 775 (399)						
6.0				1 681 (378)						

TABLE IV. - PILOT RATINGS OF AIRCRAFT HANDLING QUALITIES ON LANDING APPROACH (PRIOR TO FLARE)

Control configuration	Motion	Turbulence	EO	Average* pilot rating
FULLY AUGMENTED (Spread engines)				2
			X	2
		X		3
		X	X	3
	X			$2\frac{1}{2}$
	X	X		3
	X		X	$2\frac{1}{2}$
	X	X	X	3
BASIC + SAS (Clustered engines)				4
			X	4
		X		$4\frac{1}{2}$
		X	X	6
	X			$4\frac{1}{2}$
	X		X	5
	X	X		6
	X	X	X	7
BASIC (Clustered engines)				$7\frac{1}{2}$
			X	10
		X		10
	X			8
	X		X	10
	X	X		10

*Average for the three pilots.

TABLE V.- PILOT RATING SYSTEM

CONTROLLABLE Capable of being controlled or managed in context of mission, with available pilot attention.	ACCEPTABLE May have deficiencies which warrant improvement, but adequate for mission. Pilot compensation, if required to achieve acceptable performance, is feasible.	SATISFACTORY Meets all requirements and expectations; good enough without improvement. Clearly adequate for mission.	Excellent, highly desirable.	1
			Good, pleasant, well behaved.	2
			Fair. Some mildly unpleasant characteristics. Good enough for mission without improvement.	3
		UNSATISFACTORY Reluctantly acceptable. Deficiencies which warrant improvement. Performance adequate for mission with feasible pilot compensation.	Some minor but annoying deficiencies. Improvement is requested. Effect on performance is easily compensated for by pilot.	4
			Moderately objectionable deficiencies. Improvement is needed. Reasonable performance requires considerable pilot compensation.	5
			Very objectionable deficiencies. Major improvements are needed. Requires best available pilot compensation to achieve acceptable performance.	6
	UNACCEPTABLE Deficiencies which require improvement. Inadequate performance for mission even with maximum feasible pilot compensation.		Major deficiencies which require improvement for acceptance. Controllable. Performance inadequate for mission, or pilot compensation required for minimum acceptable performance in mission is too high.	7
			Controllable with difficulty. Requires substantial pilot skill and attention to retain control and continue mission.	8
			Marginally controllable in mission. Requires maximum available pilot skill and attention to retain control.	9
UNCONTROLLABLE Control will be lost during some portion of mission.			Uncontrollable in mission.	10

TABLE VI.- RESULTS OF EO RECOVERY (IFR) AND TOUCHDOWN WITH FULL AUGMENTATION

	Fixed base		Moving base			
	Smooth air (16 tests)		Smooth air (14 tests)		Turbulence (10 tests)	
Recovery:						
Mean $(\epsilon_h)_{EO}$	4.10 m	13.44 ft	4.83 m	15.86 ft	4.51 m	14.80 ft
Standard deviation	1.34 m	4.40 ft	2.30 m	7.54 ft	2.57 m	8.42 ft
Mean $(\Delta Y)_{EO}$	6.40 m	21.00 ft	6.95 m	22.79 ft	8.72 m	28.60 ft
Standard deviation	3.95 m	12.96 ft	4.29 m	14.08 ft	4.98 m	16.35 ft
Touchdown[a]:						
Mean X	160.32 m	526 ft	155.14 m	509 ft	131.98 m	433 ft
Standard deviation	40.84 m	134 ft	53.64 m	176 ft	67.97 m	223 ft
Mean Y	7.37 m	24.19 ft	7.58 m	24.86 ft	5.04 m	16.55 ft
Standard deviation	6.55 m	21.50 ft	5.02 m	16.46 ft	3.58 m	11.75 ft
Mean rate of descent	1.26 m/sec	4.13 ft/sec	1.77 m/sec	5.80 ft/sec	2.21 m/sec	7.25 ft/sec
Standard deviation	.53 m/sec	1.74 ft/sec	.66 m/sec	2.15 ft/sec	1.24 m/sec	4.07 ft/sec
Flare initiation[b]:						
Mean rate of descent	3.81 m/sec	12.49 ft/sec	3.63 m/sec	11.90 ft/sec	3.68 m/sec	12.07 ft/sec
Standard deviation	.25 m/sec	.81 ft/sec	.55 m/sec	1.80 ft/sec	.53 m/sec	1.75 ft/sec

[a]Designated touchdown zone, $76.2 \text{ m} \leq X \leq 213.4 \text{ m}$ ($250 \text{ ft} \leq X \leq 700 \text{ ft}$).

[b]Nominal rate of descent, 4 m/sec (13.23 ft/sec).

Weight, N (lbf)	245 096 (55 100)
Wing area, m^2 (ft^2)	78 (843)
Wing span, m (ft)	24 (78)
Mean aerodynamic chord, $\bar{c}$, m (ft)	3.58 (11.74)
Center-of-gravity location, percent $\bar{c}$	40
I_X, kg-m^2 (slug-ft^2)	331 102 (244 212)
I_Y, kg-m^2 (slug-ft^2)	334 637 (246 819)
I_Z, kg-m^2 (slug-ft^2)	625 677 (461 482)
I_{XZ}, kg-m^2 (slug-ft^2)	27 690 (20 423)

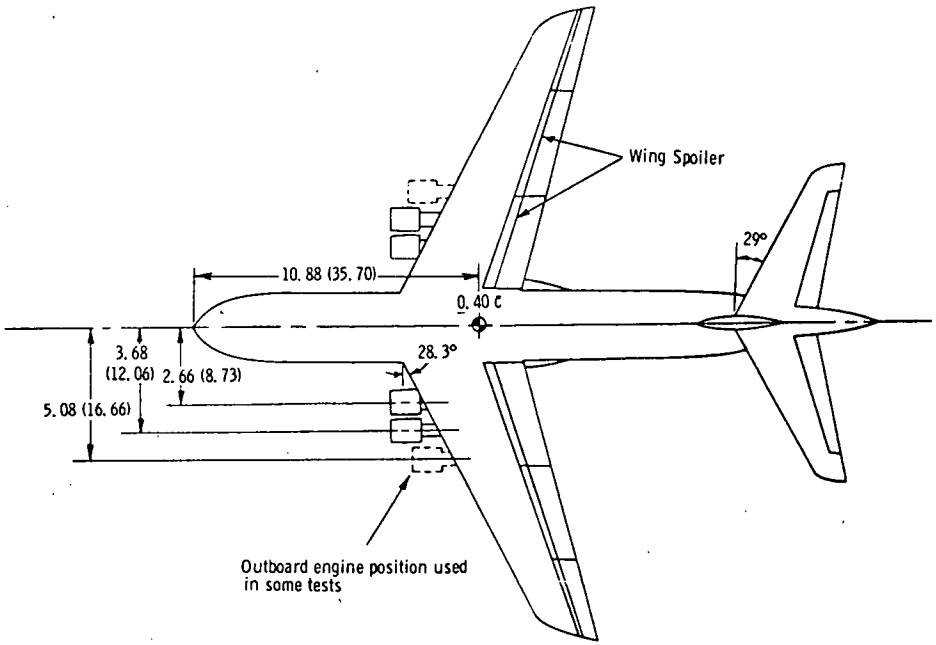

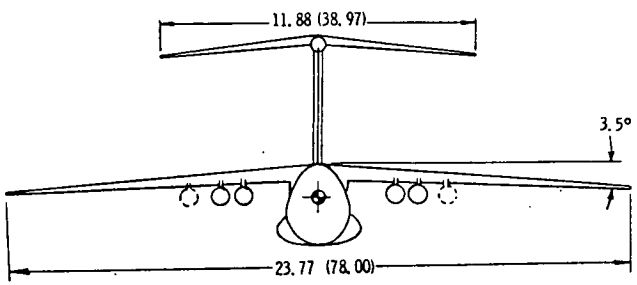

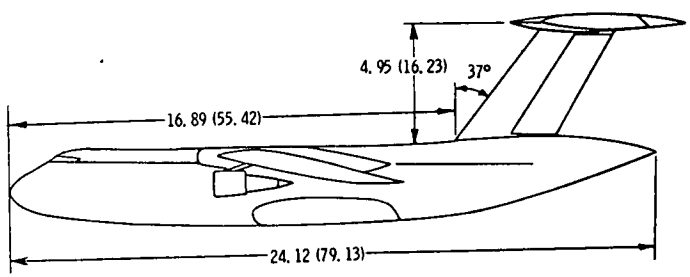

Figure 1.- Three-view drawing of simulated airplane. All linear dimensions are in m (ft).

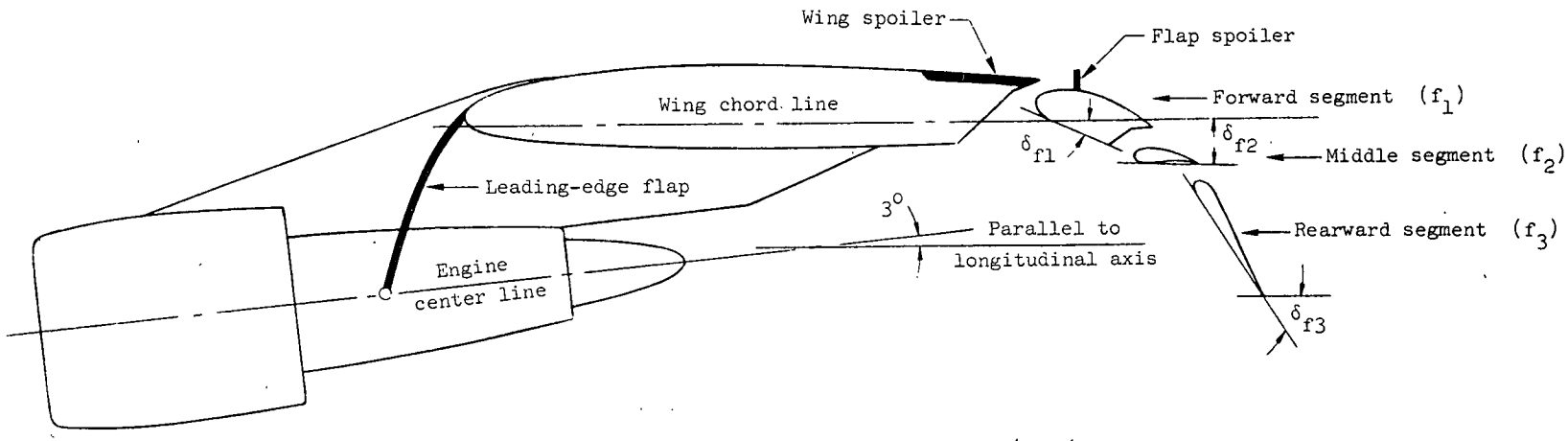

Figure 2.- Flap assembly and engine pylon detail. $\delta_{f1}/\delta_{f2}/\delta_{f3} = 25°/10°/60°$.

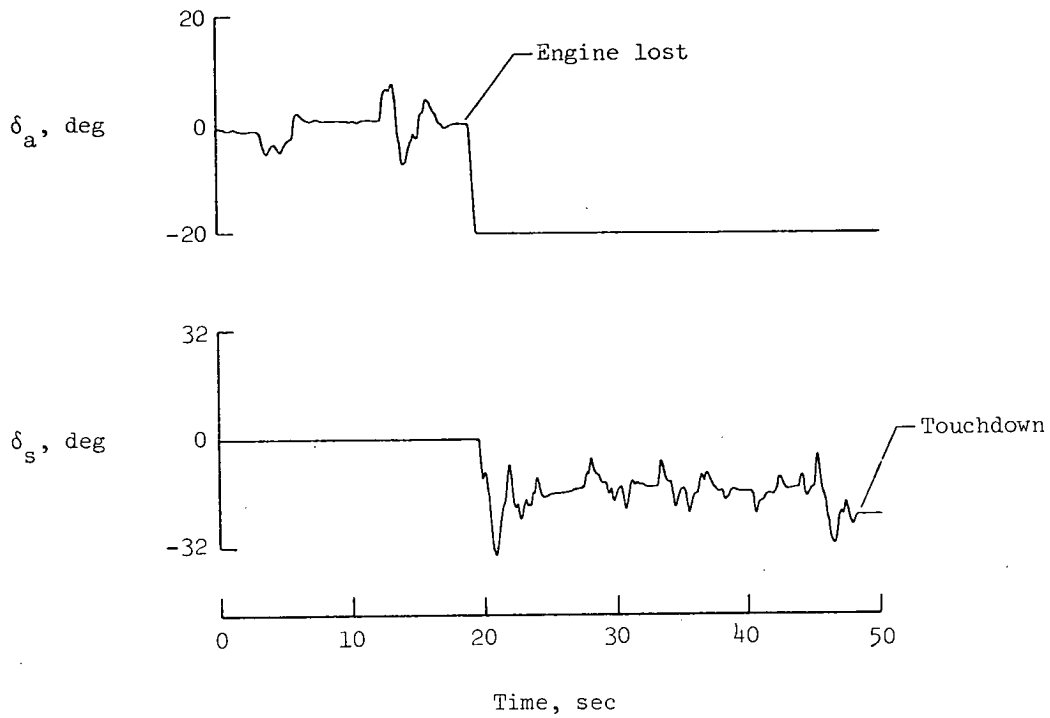

Figure 3.- Typical response of ailerons and spoilers to failure of outboard engine on right wing.

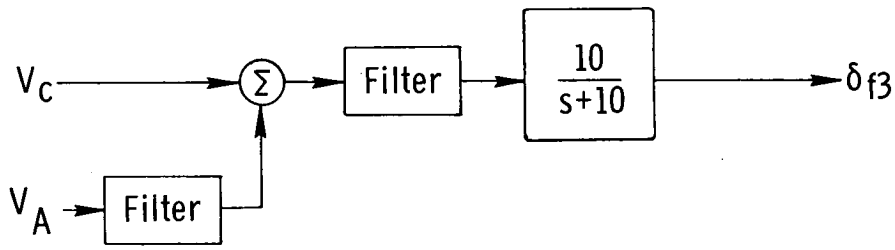

Figure 4.- Automatic speed control (AUTOSPEED).

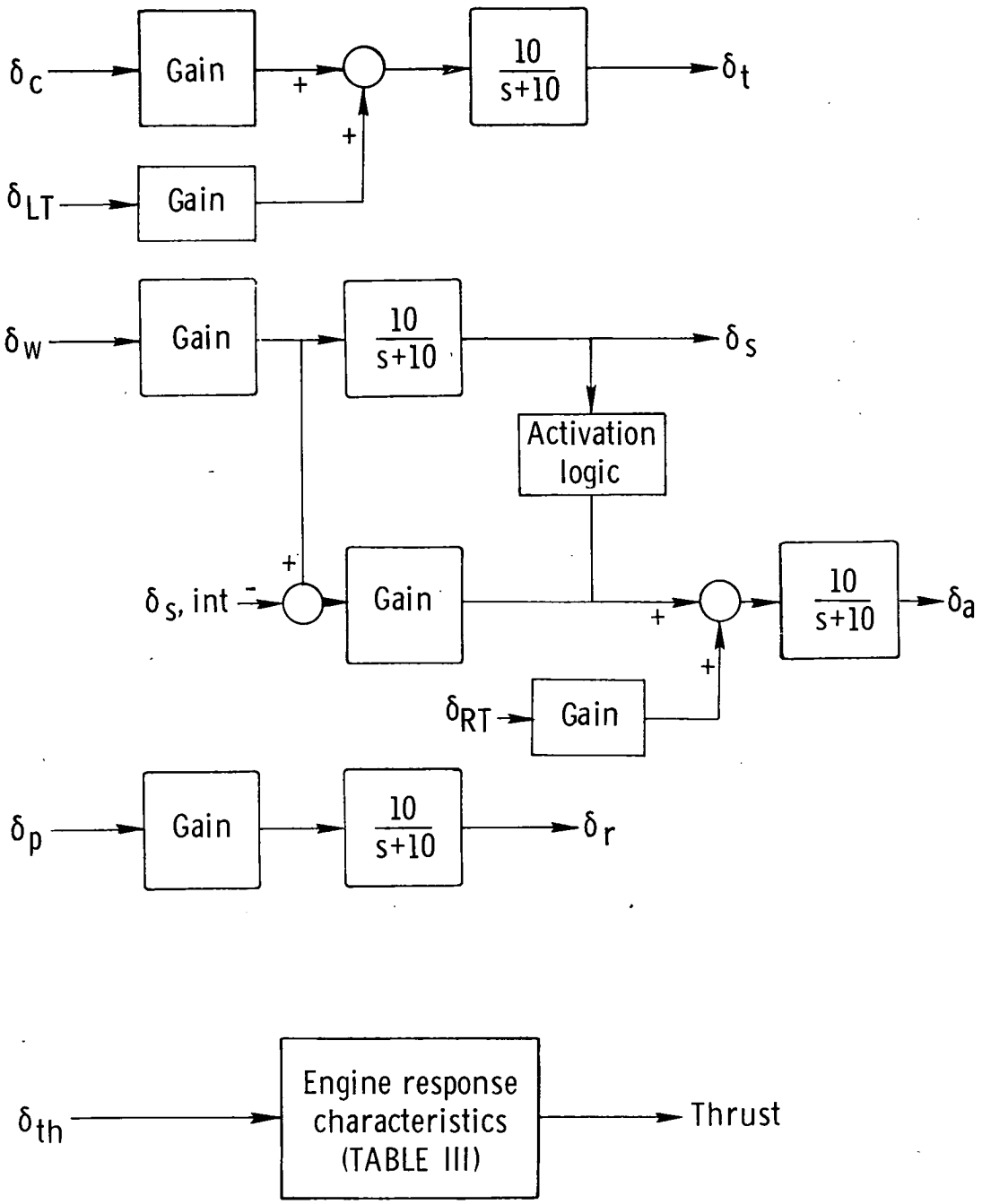

Figure 5.- Basic flight controls.

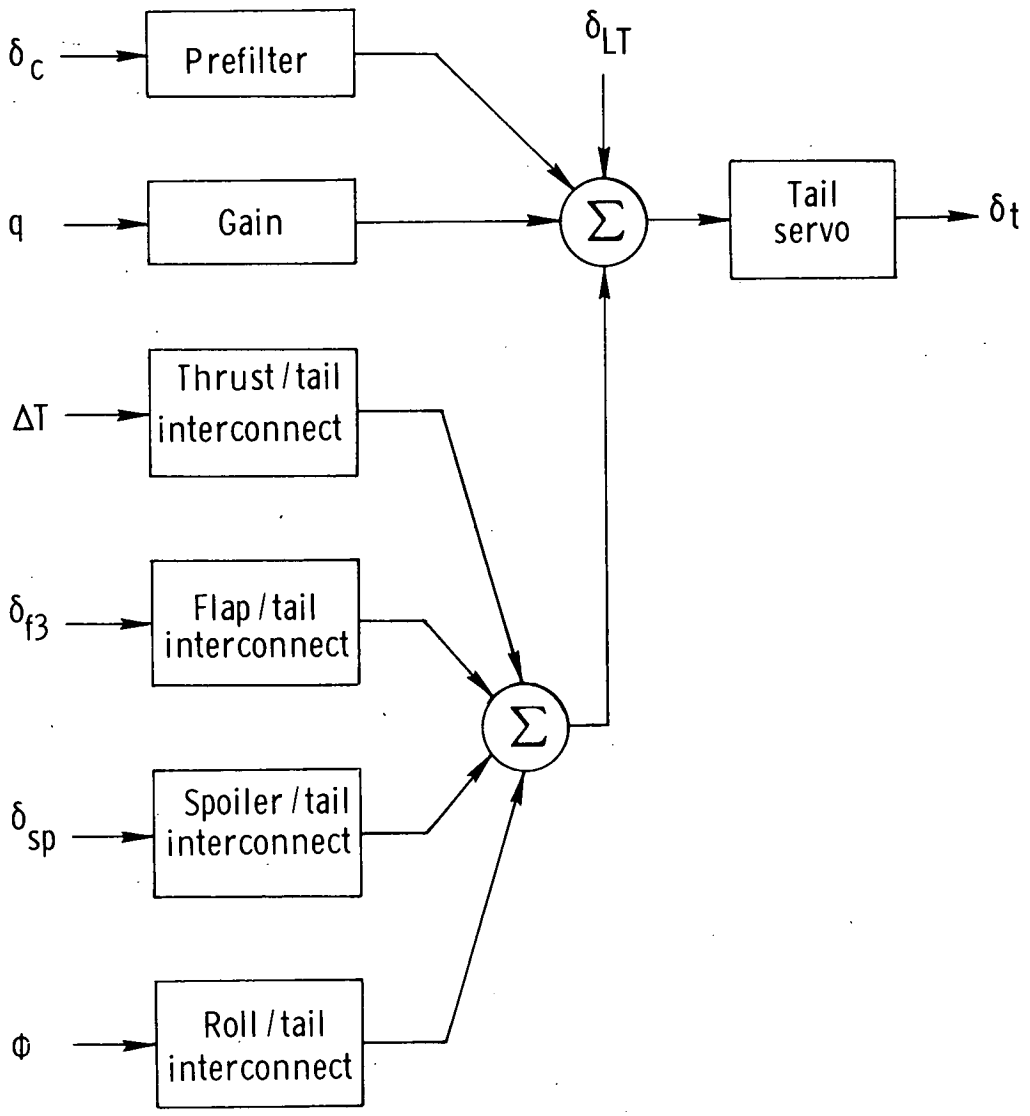

Figure 6.- Basic longitudinal augmentation.

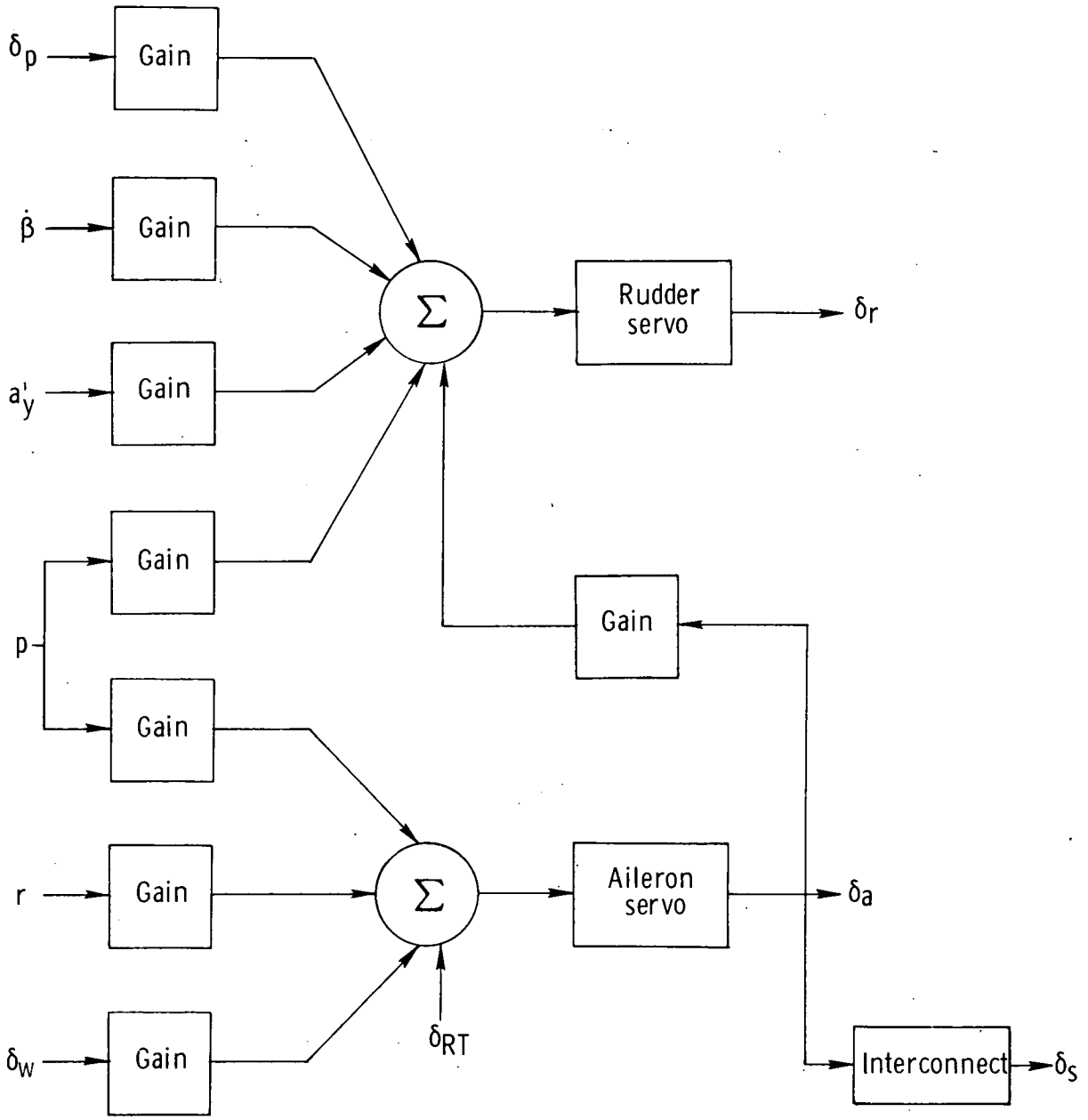

Figure 7.- Basic lateral-directional augmentation.

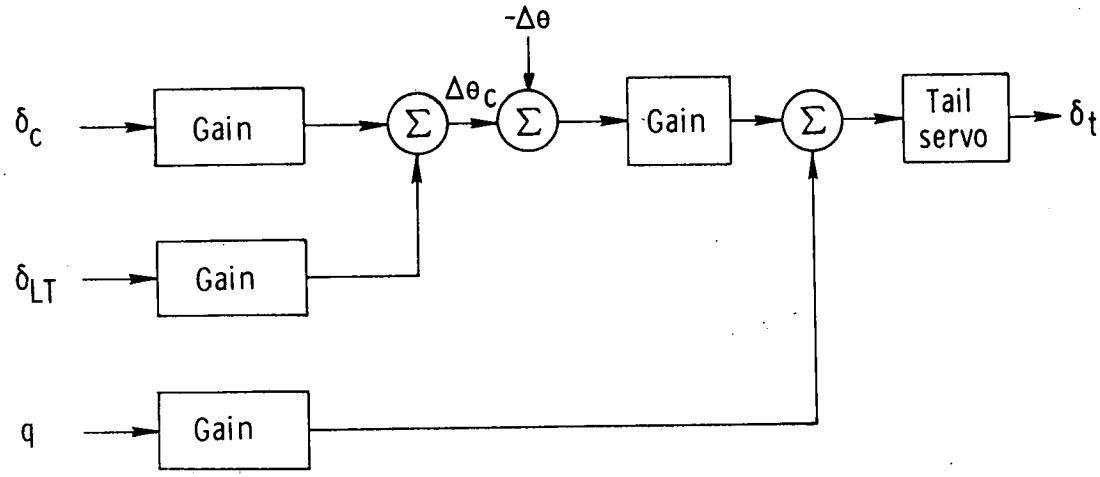

(a) Pitch-attitude command system ($\Delta\theta$ denotes pitch angle error and $\Delta\theta_c$ denotes commanded pitch angle change).

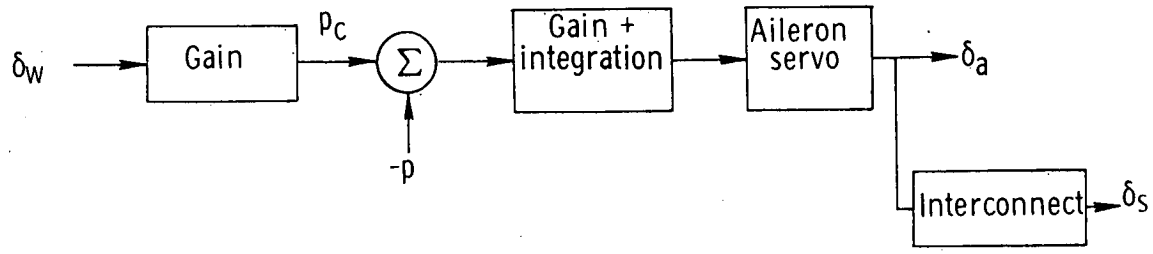

(b) Roll-rate command system (p_c denotes commanded roll rate).

Figure 8.- Command augmentation systems.

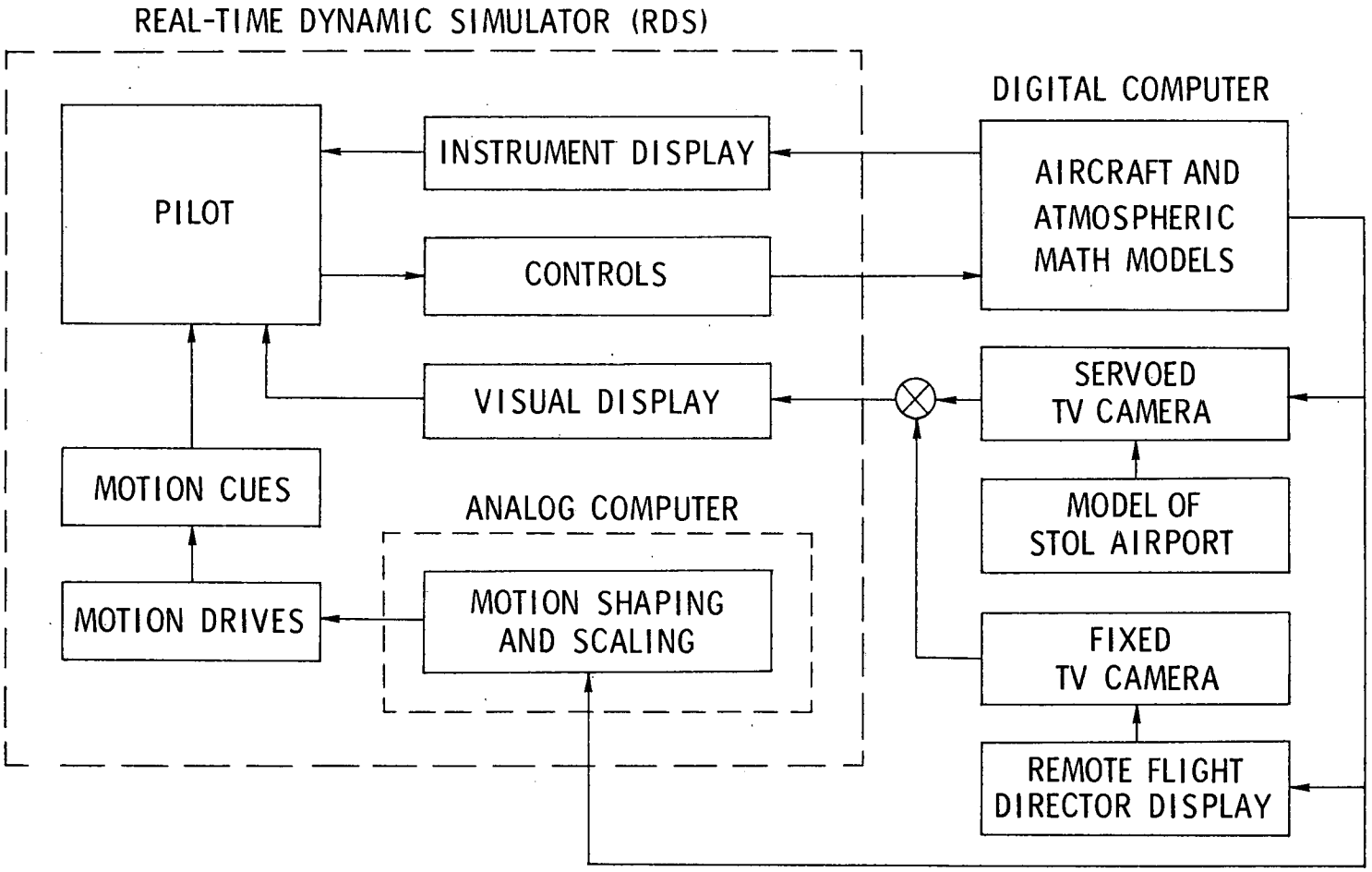

Figure 9.- RDS/STOL simulation system.

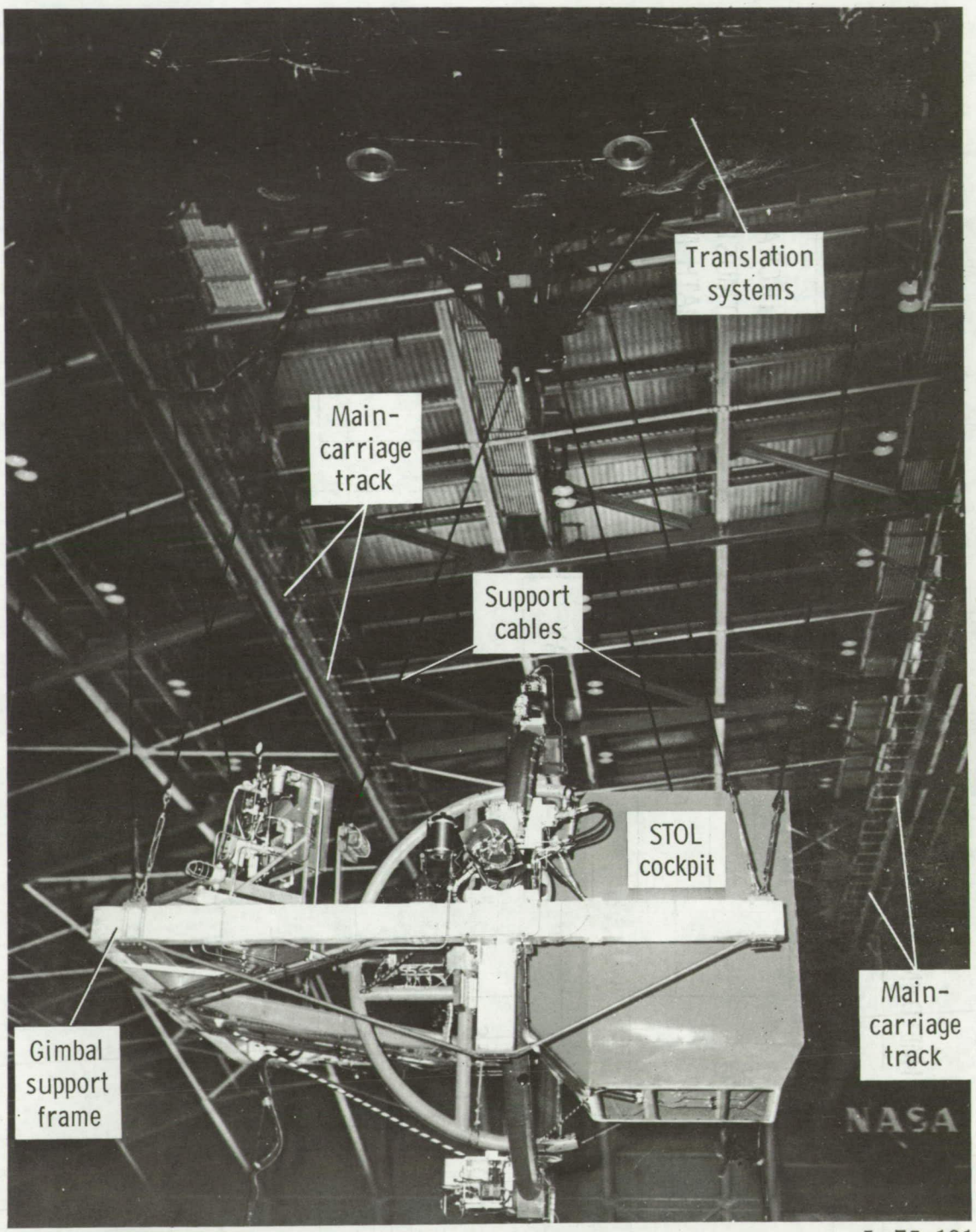

L-75-181

Figure 10.- Real-time dynamic simulator (RDS) with STOL cockpit mounted in the gimbals.

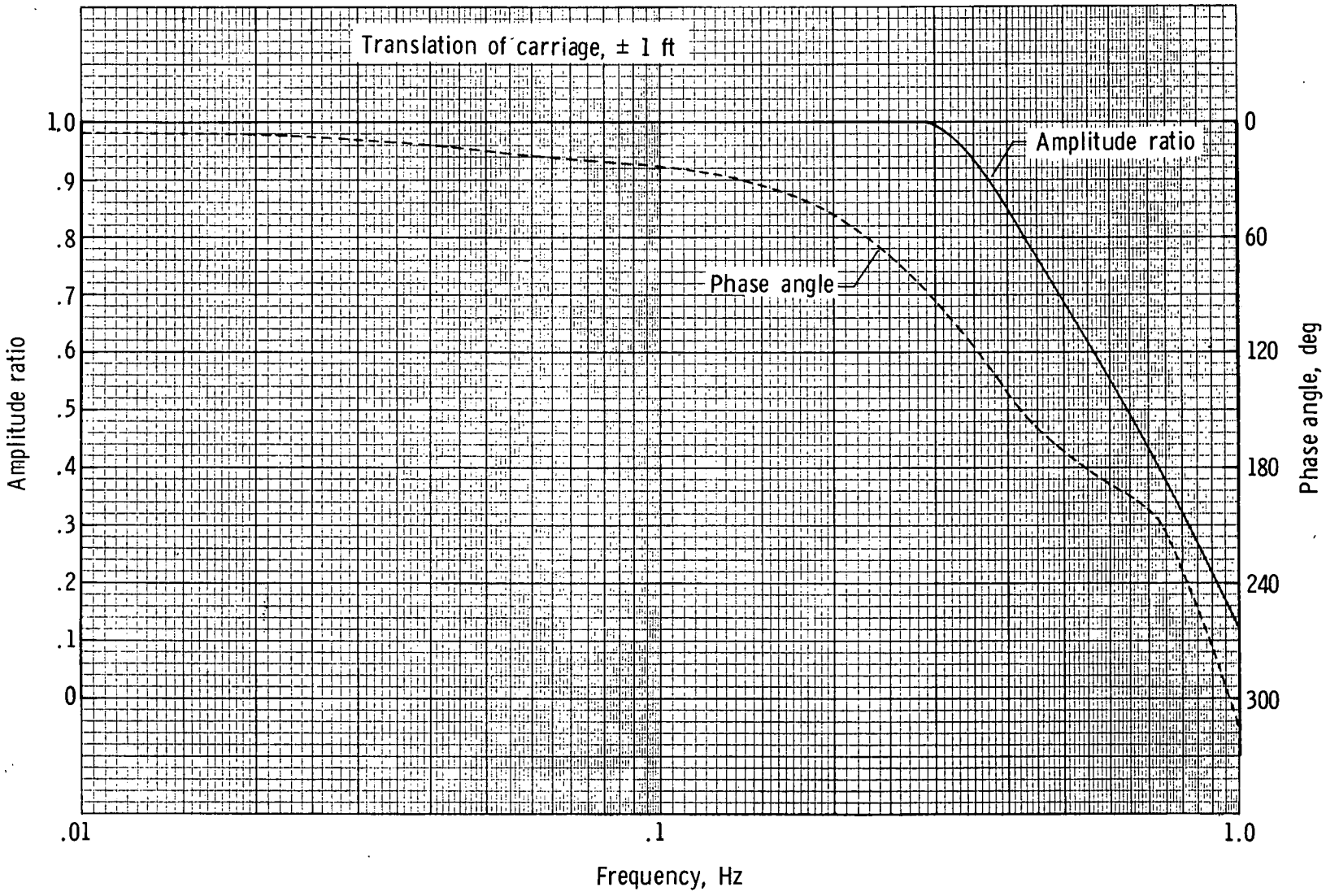

Figure 11.- Typical example of the frequency response of the RDS.

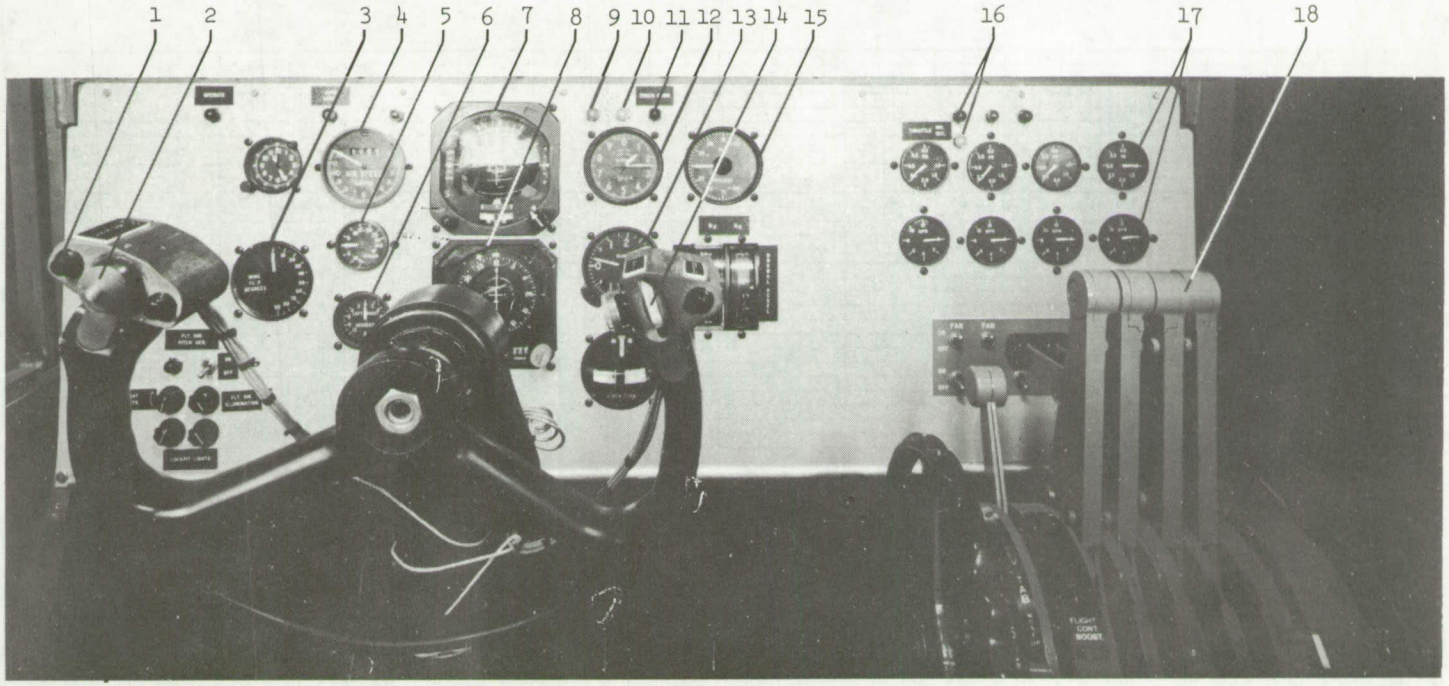

1 Autospeed button
2 Pitch and roll trim
3 δ_{f3} flap deflection
4 Airspeed
5 Angle of attack
6 Angle of sideslip
7 Flight dir. and attitude ind.
8 Horizontal situation indicator
9 Flare warning light
10 Flare initiation light
11 Touchdown light
12 Altimeter
13 Rate of climb
14 Direct-lift-control wheel
15 Direct-lift-control meter
16 Thrust trim lights
17 Engine instruments
18 Throttles

L-75-182

Figure 12.- Pilot's view of cockpit interior.

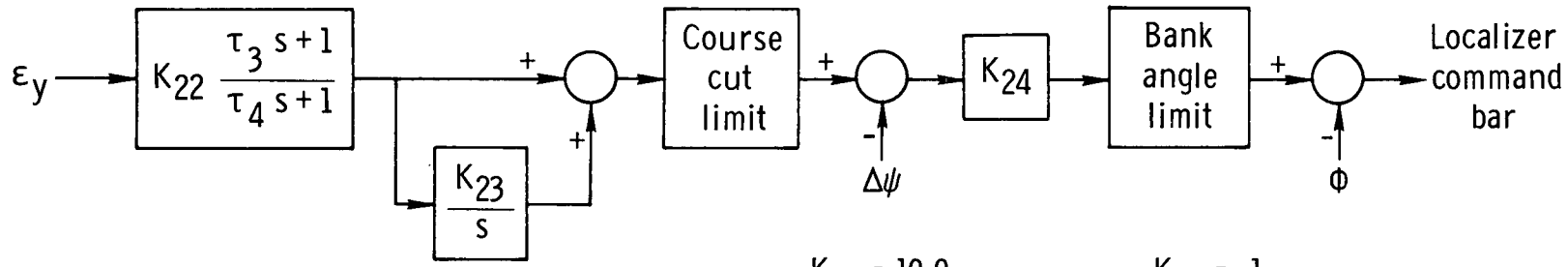

$K_{22} = 10.0$

$\tau_3 = 2.86$ sec

$\tau_4 = 0.2$ sec

$K_{24} = 1$

$K_{23} = \begin{cases} 0.10\ \text{sec}^{-1}, & \varepsilon_y \leq 0.3 \\ 0, & \varepsilon_y > 0.3 \end{cases}$

(a) Localizer channel.

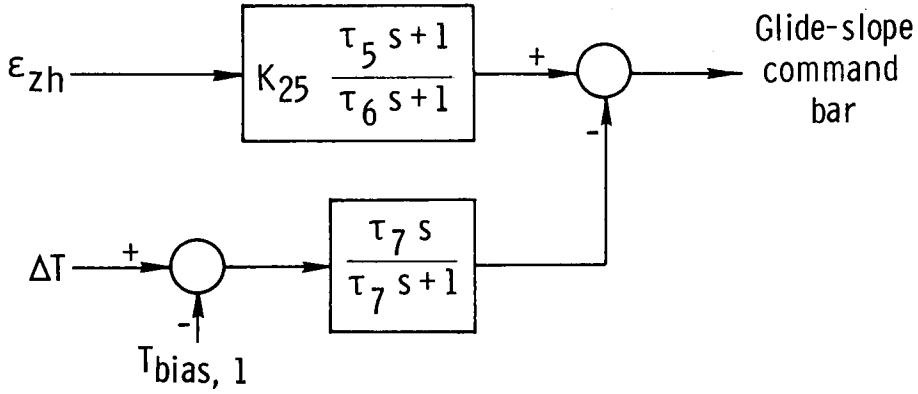

$K_{25} = 2.64$ kN/m (181 lbf/ft)

$\tau_5 = 3.33$ sec

$\tau_6 = 0.4$ sec

$\tau_7 = 10$ sec

(b) Glide-slope channel.

Figure 13.- Flight director command bar drive signals.

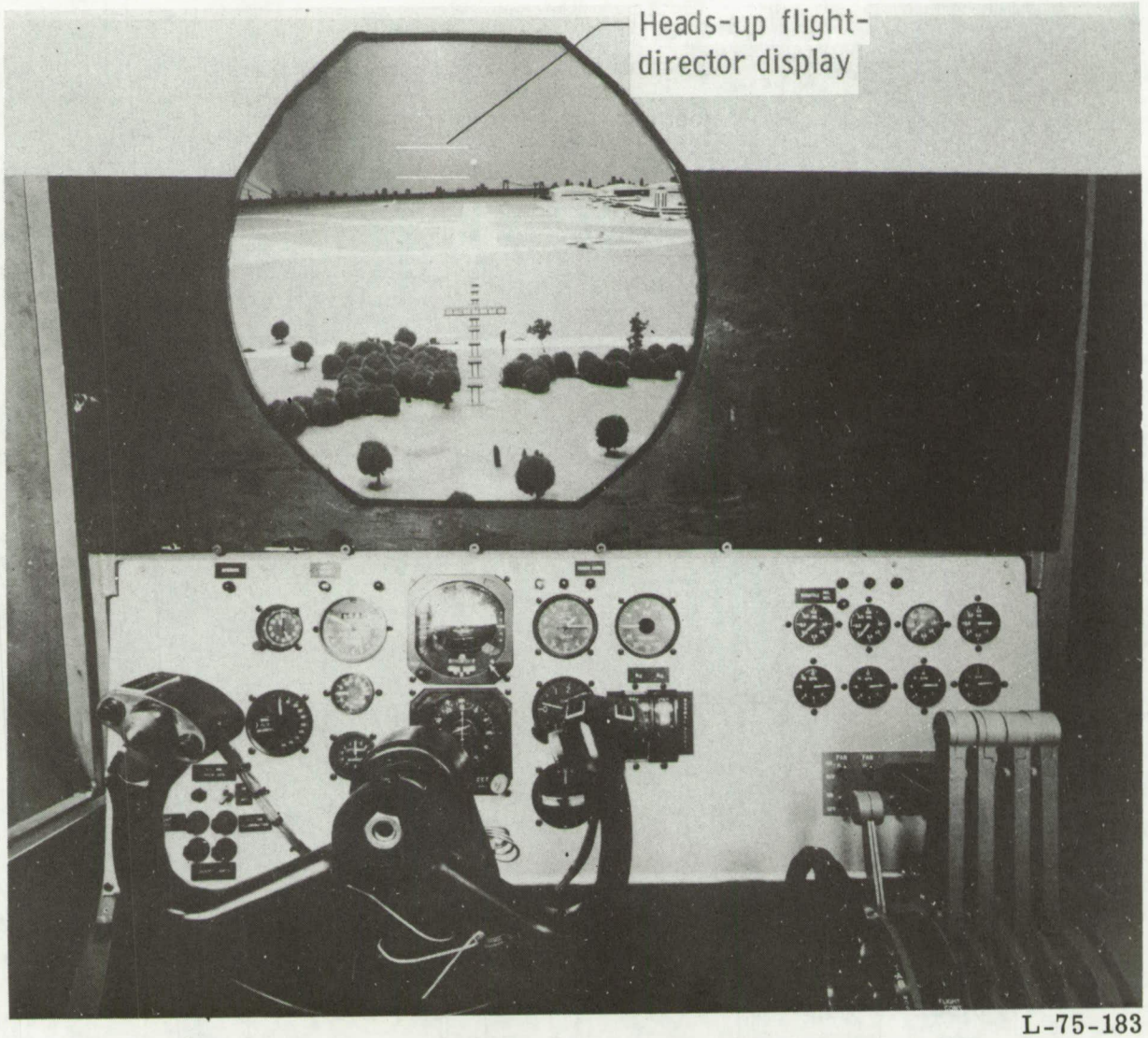

L-75-183

Figure 14.- Pilot's view of STOL airport through virtual image lens windshield.

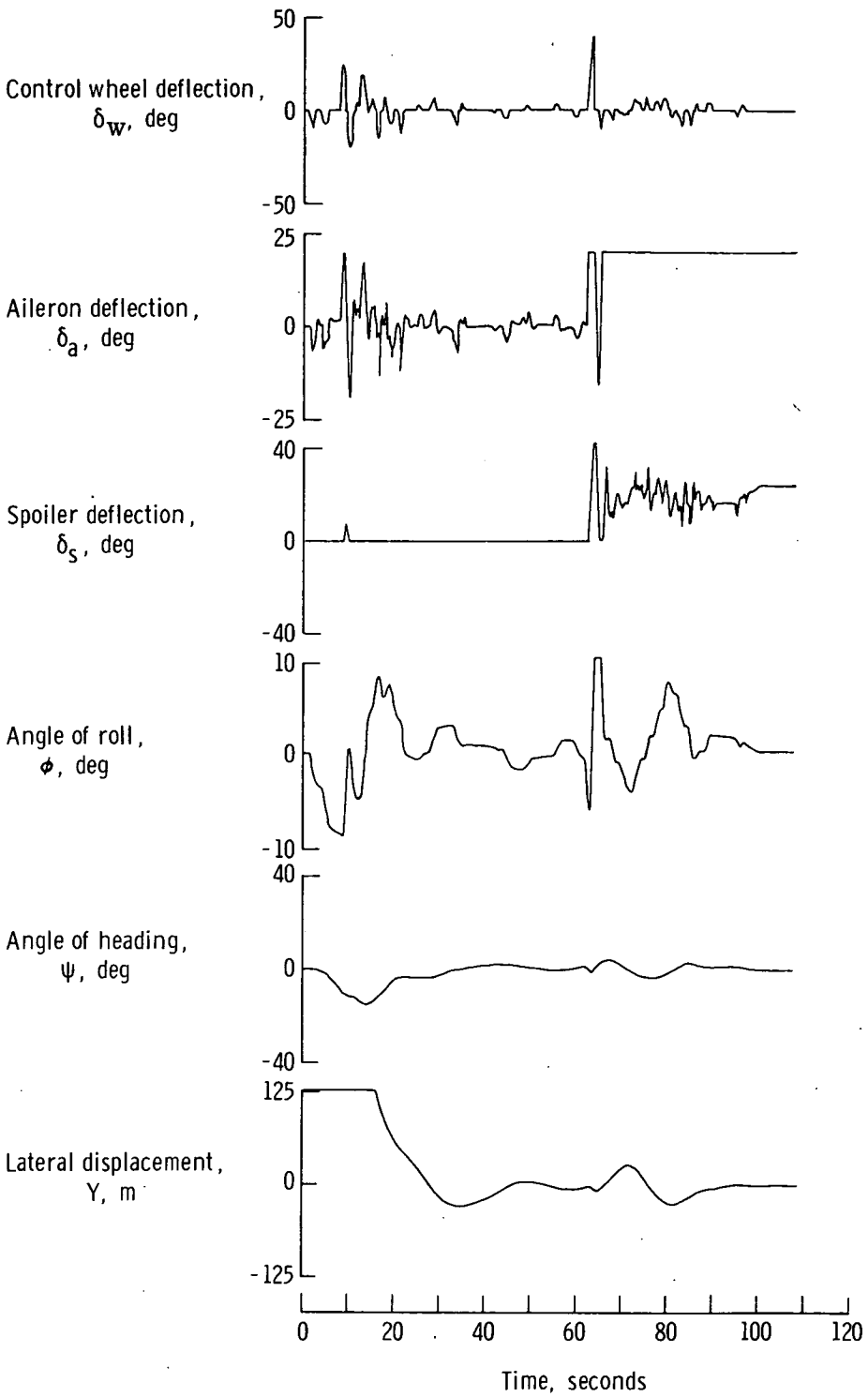

Figure 15.- A typical time history of the lateral-directional variables during an approach involving an engine failure.

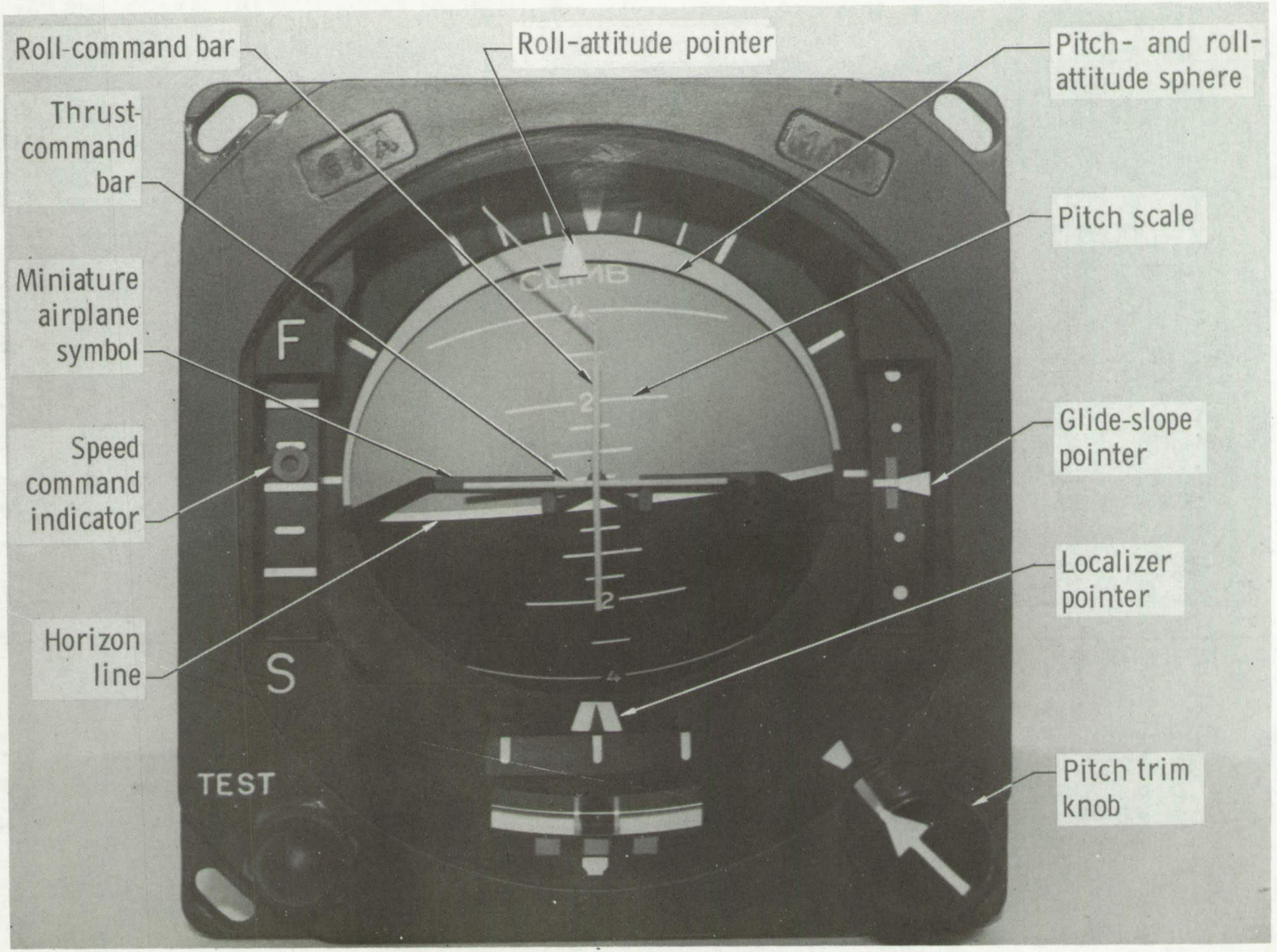

L-73-4451.1

Figure 16.- Flight director and attitude indicator.

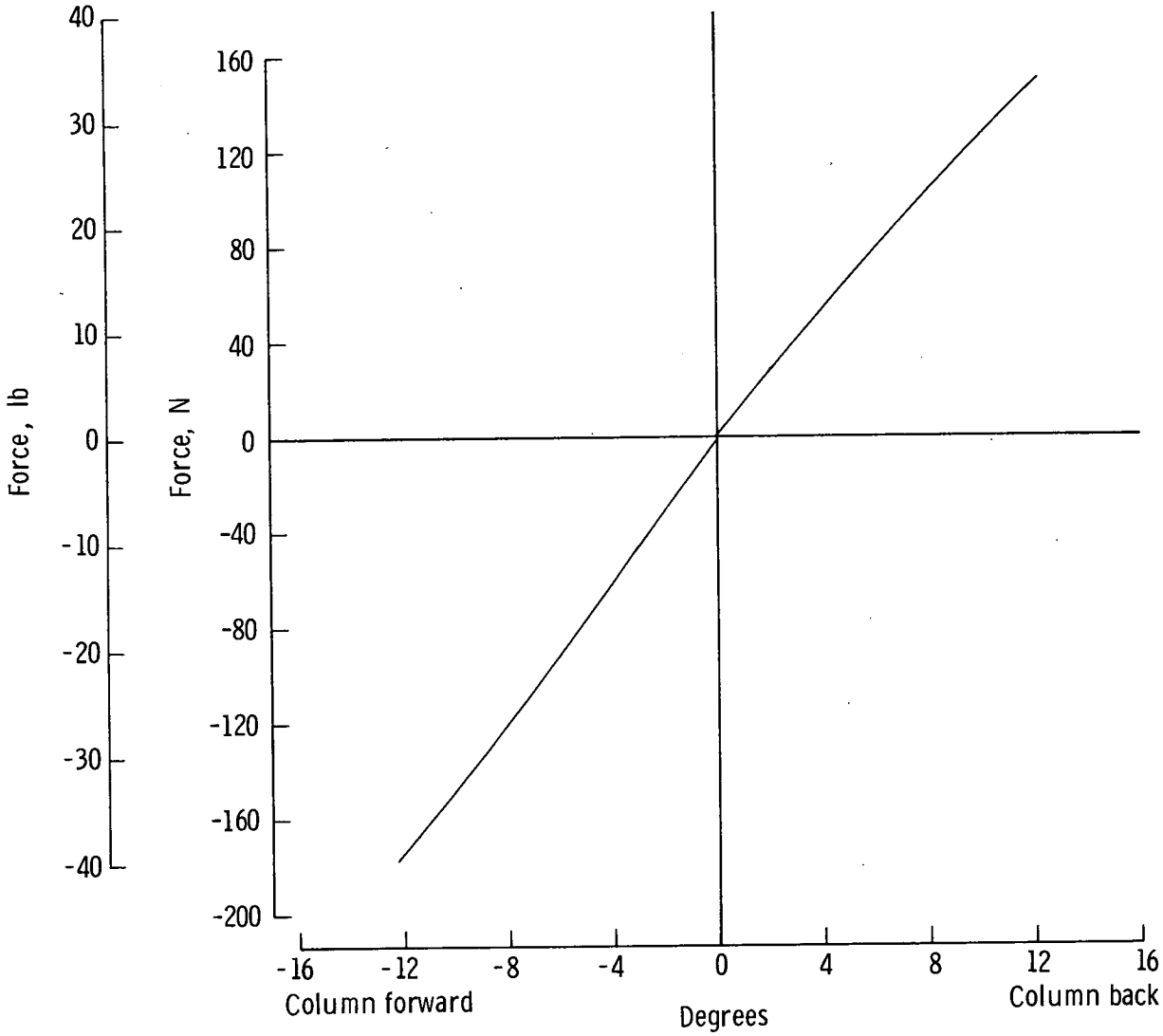

Figure 17.- Column force-deflection curve.

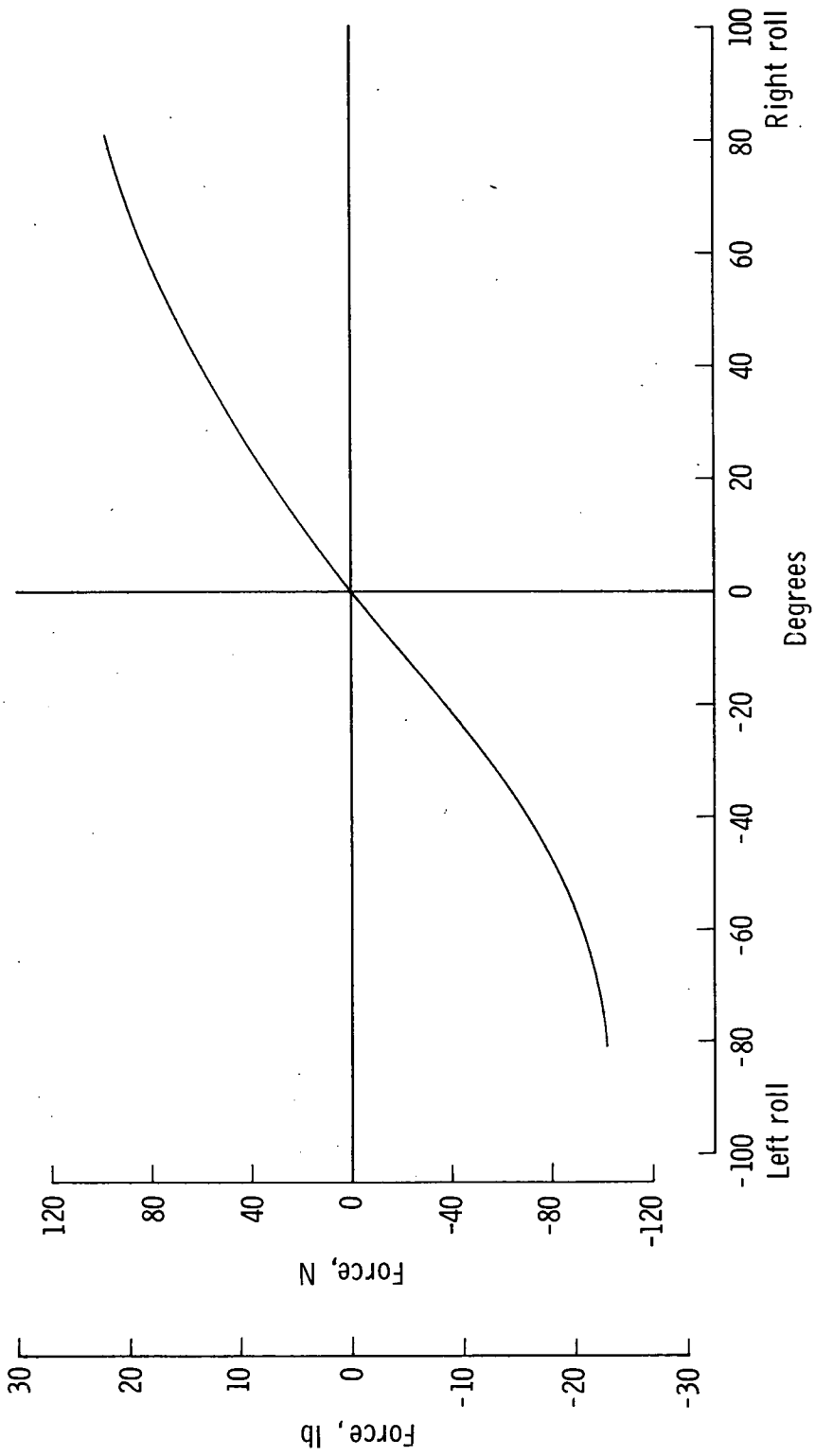

Figure 18.- Wheel force-deflection curve.

NASA-Langley, 1975

"The aeronautical and space activities of the United States shall be conducted so as to contribute . . . to the expansion of human knowledge of phenomena in the atmosphere and space. The Administration shall provide for the widest practicable and appropriate dissemination of information concerning its activities and the results thereof."

—NATIONAL AERONAUTICS AND SPACE ACT OF 1958

NASA SCIENTIFIC AND TECHNICAL PUBLICATIONS

TECHNICAL REPORTS: Scientific and technical information considered important, complete, and a lasting contribution to existing knowledge.

TECHNICAL NOTES: Information less broad in scope but nevertheless of importance as a contribution to existing knowledge.

TECHNICAL MEMORANDUMS: Information receiving limited distribution because of preliminary data, security classification, or other reasons. Also includes conference proceedings with either limited or unlimited distribution.

CONTRACTOR REPORTS: Scientific and technical information generated under a NASA contract or grant and considered an important contribution to existing knowledge.

TECHNICAL TRANSLATIONS: Information published in a foreign language considered to merit NASA distribution in English.

SPECIAL PUBLICATIONS: Information derived from or of value to NASA activities. Publications include final reports of major projects, monographs, data compilations, handbooks, sourcebooks, and special bibliographies.

TECHNOLOGY UTILIZATION PUBLICATIONS: Information on technology used by NASA that may be of particular interest in commercial and other non-aerospace applications. Publications include Tech Briefs, Technology Utilization Reports and Technology Surveys.

Details on the availability of these publications may be obtained from:

SCIENTIFIC AND TECHNICAL INFORMATION OFFICE

NATIONAL AERONAUTICS AND SPACE ADMINISTRATION

Washington, D.C. 20546